

SPRAY ROLLING OF RAPIDLY SOLIDIFIED Al-Fe-V-Si ALLOY

A THESIS SUBMITTED TO
THE GRADUATE SCHOOL OF NATURAL AND APPLIED SCIENCES
OF
MIDDLE EAST TECHNICAL UNIVERSITY

BY

HALİT AKIN ÖZYURDA

IN PARTIAL FULFILLMENT OF THE REQUIREMENTS
FOR
THE DEGREE OF MASTER OF SCIENCE
IN
METALLURGICAL AND MATERIALS ENGINEERING

MAY 2006

Approval of the Graduate School of Natural and Applied Sciences

Prof. Dr. Canan ÖZGEN
Director

I certify that this thesis satisfies all the requirements as a thesis for the degree of Master of Science

Prof. Dr. Tayfur ÖZTÜRK
Head of Department

This is to certify that we have read this thesis and that in our opinion it is fully adequate, in scope and quality, as a thesis for the degree of Master of Science.

Prof. Dr. Ali KALKANLI
Supervisor

Examining Committee Members

Prof. Dr. Rıza GÜRBÜZ (METU, METE) _____

Prof. Dr. Ali KALKANLI (METU, METE) _____

Prof. Dr. Cevdet KAYNAK (METU, METE) _____

Assoc. Prof. Dr. C. Hakan GÜR (METU, METE) _____

Prof. Dr. Tamer ÖZDEMİR (GAZI UNV.) _____

I hereby declare that all information in this document has been obtained and presented in accordance with academic rules and ethical conduct. I also declare that, as required by these rules and conduct, I have fully cited and referenced all material and results that are not original to this work.

Name, Last name : Halit Akın ÖZYURDA

Signature :

ABSTRACT

SPRAY ROLLING OF RAPIDLY SOLIDIFIED Al-Fe-V-Si ALLOY

ÖZYURDA, Halit Akin

Ms.Sc. Department of Metallurgical and Materials Engineering

Supervisor: Prof. Dr. Ali KALKANLI

May 2006, 78 pages

In this study an experimental spray-rolling set-up is designed in order to produce rapidly solidified Al-Fe-V-Si flat product. Al-Fe-V-Si alloys produced by rapid solidification powder metallurgy (RSP/M) methods are mostly used in high temperature applications in aerospace and automotive industries. The RSP/M technique used is spray deposition, which is desirable because of the high cooling rates achieved, as a result fine silicide dispersoids and intermetallics are observed in the microstructure which are known to contribute to the mechanical properties i.e. high strength at elevated temperatures, thermal stability, fracture toughness, corrosion resistance. Since spray deposition is a droplet consolidation process a considerable amount of porosity is expected in the final product. In this work, spray rolling process, which consists of spray deposition and subsequent hot twin-rolling stage, is designed and developed by interpreting the results obtained from SEM, XRD, tensile, three point bending and hardness tests of the specimens formed in several design stages. Two original intermetallic phases characterized in this study are V_3Si and $V_2Mg_3Al_{18}$.

Keywords: AlFeVSi alloy, spray rolling method, rapid solidification, spray deposition

ÖZ

HIZLI KATILAŞMIŞ Al-Fe-V-Si ALAŞIMININ PÜSKÜRTME HADDELENMESİ

ÖZYURDA, Halit Akın

Yüksek Lisans, Metalurji ve Malzeme Mühendisliği Bölümü

Tez Yöneticisi: Prof. Dr. Ali KALKANLI

Mayıs 2006, 78 sayfa

Bu çalışmada hızlı katılaşımiş düz şerit halinde AlFeVSi alaşımı ürününün üretilmesini hedefleyen deneysel bir püskürtme haddeleme düzeneği tasarlanmaktadır. Hızlı katılma toz metalürjisi (HKT/M) yöntemleriyle üretilen AlFeVSi alaşımları ağırlıkla uçak ve otomotiv endüstrisinde yüksek sıcaklıktaki uygulamalarda kullanılırlar. Bu çalışmada HKT/M yöntemi olarak püskürtme biriktirme kullanılmıştır. Püskürtme biriktirme yöntemi, yüksek sıcaklıklardaki güç, termal kararlılık, kırılma tokluğu, korozyon dayancısı gibi mekanik özelliklere katkıda bulunduđu bilinen ince silisid tanecikleri ve intermetaliklerin içyapıda gözlenmesini sağlayan yüksek soğuma hızlarına ulaşılabilirdiği için istenmiştir. Püskürtme biriktirmenin bir damlacık yoğunlaştırma yöntemi olmasından dolayı son üründe gözeneklilik beklenmektedir. Bu çalışmada, püskürtme biriktirme sürecini takiben bir sıcak çift haddeleme aşamasından oluşan püskürtme haddeleme süreci, tasarım aşamalarından elde edilen numunelerin SEM, XRD, çekme, üç nokta bükme ve sertlik değerlendirmelerinden elde edilen sonuçların yorumlanması ile tasarlanacak ve geliştirilecektir. Bu çalışmada tanımlanan özgün intermetallic fazları V_3Si ve $V_2Mg_3Al_{18}$ 'dir.

Anahtar Kelimeler: AlFeVSi alaşımı, püskürtme haddeleme yöntemi, hızlı katılma, püskürtme döküm

To My Family

ACKNOWLEDGEMENTS

I would like to express my deepest gratitude and appreciation to my supervisor Prof. Dr. Ali Kalkanlı for his support, inspiration, motivation, criticism and excellent guidance since my graduation project.

I would also like to express my great thanks my co-worker Kağan Menekşe for his support, ideas and friendship.

I would like to express my special thanks to the Mastırkastır Team (Kağan Menekşe, Arda Çetin, Salih Türe and Ufuk Cengizel) for their assistance and friendship through the experimental work of this study.

I would like express my sincere thanks to my parents; Ümit - Ferda Özyurda and my sister Deniz for their never-ending love, support, motivation and guidance during this study and during my life.

Finally, I would like to thank Sahir Gül, Mehmet Oğuz and Müfit Özyurda for their support, understanding and motivation during this study.

TABLE OF CONTENTS

PLAGIARISM.....	iii
ABSTRACT.....	iv
ÖZ.....	v
DEDICATION.....	vi
ACKNOWLEDGEMENTS.....	vii
TABLE OF CONTENTS.....	viii

CHAPTERS

1. INTRODUCTION.....	1
2. THEORY AND LITERATURE SURVEY.....	3
2.1 Elevated Temperature Aluminum Alloys.....	3
2.2 Rapidly Solidified Al-Fe-V-Si Alloy.....	5
2.3 Spray Deposition.....	7
2.3.1 Features and History of Spray Deposition.....	7
2.3.2 Fundamentals of Spray Deposition.....	10
2.4 Spray Rolling.....	14
3. EXPERIMENTAL PROCEDURE.....	17
3.1 Alloy Preparation and Composition.....	17
3.2 Spray Rolling Set-up Design.....	18

3.2.1 Early Spray Rolling Setups' Design Stages.....	20
3.2.2 Advanced Design of Spray Rolling Setup.....	25
3.3 Hot Rolling.....	32
3.4 X-Ray Diffraction Study.....	32
3.5 Optical and Scanning Electron Microscopy Study.....	32
3.6 Hardness Test.....	33
3.7 Three Point Bending Test.....	33
3.8 Tensile Test.....	34
3.9 True Density Measurement Study.....	34
4. RESULTS AND DISCUSSION.....	35
4.1 Phase Characterization.....	35
4.1.1 Optical and Scanning Electron Microscopy Results.....	36
4.1.2 X-Ray Diffraction Results.....	54
4.2 Mechanical Test Results.....	58
4.2.1 Three Point Bending Test Results.....	58
4.2.2 Tensile Test Results.....	60
4.2.3 Hardness Test Results.....	61
4.3 True Density Measurement Results.....	63
5. CONCLUSIONS.....	64
6. SUGGESTIONS FOR FUTURE WORK.....	66
REFERENCES.....	67
APPENDICES.....	72
A: X-RAY DIFFRACTION CARDS OF THE CHARACTERIZED PHASES.	72
B: SAMPLE STRESS VS STRAIN GRAPH OF B2 SPECIMEN.....	78

CHAPTER1

INTRODUCTION

In this study a 8009 series aluminum alloy is concerned which has the alloying elements Fe, V and Si. This alloy is designed by Allied Signal Inc. in the 1980s [6]. The alloy is designed by the addition of V to the Al-Fe-Si ternary alloy, the vanadium addition showed that when processed by rapid solidification a fine silicide dispersiod phase is stabilized in the microstructure giving the alloy exceptional room and elevated temperature properties.

The rapid solidification processing which is necessary in production of Al-Fe-V-Si alloys is mostly applied by powder metallurgy routes including the powder production and consolidation steps. The main objective of this study is to assess the production of the Al-Fe-V-Si with a different process than the conventional powder metallurgy route, namely the spray rolling which consists of two main stages spray deposition of the molten alloy for rapid solidification and subsequent hot rolling for the simultaneous consolidation of the end product in the same process. This process is firstly introduced by A.R.E. Singer in 1970s [18,19,22] and substantially developed until present. The attempt to use the spray rolling process for the production of Al-Fe-V-Si alloy is believed to result in valuable data and contribution when the properties of related alloy resulting from rapid solidification is concerned.

The process design of spray rolling of Al-Fe-V-Si alloy is carried out by control of the process parameters together with the interpreting of the results obtained from the process design stages by the usage of testing and characterization tools as scanning electron microscopy, X-ray diffraction and mechanical tests like tensile, three point bending, hardness. The conclusions derived from the analysis of the process by assessment of results obtained from the mentioned tools, are used for evolution of the laboratory scale experimental spray-rolling set-up.

CHAPTER 2

THEORY AND LITERATURE SURVEY

2.1 Elevated Temperature Aluminum Alloys

Powder metallurgy technology is inherently appropriate for designing alloys for elevated temperature service. Rapid solidification conditions attained by powder metallurgy technology allows the formation of finely dispersed intermetallic strengthening phases which give resistance to coarsening and are not practical, or in some situations not possible to be formed by conventional ingot metallurgy methods.

Early studies on the elevated temperature aluminum alloy design were aiming the service temperature as 315 to 345°C. But in 1980s U.S. Air Force extended the possible service temperature to a challenging state of 480°C. Much of the development in this area is achieved by dispersing slow-diffusivity transition metals as intermetallic phases in aluminum and most of the alloys developed contain iron. [1]

Scientists of Alcoa investigated numerous alloys and they designed the commercial Al-Fe-Ce alloys for elevated temperature service with the designations of CU78 and CZ42. These alloys show good tensile strength up to 315°C and also good room temperature properties after exposed to elevated temperatures. [2,3,4] It is also reported that these alloys also has good resistance to environmentally assisted cracking. [4]

The leading RS-P/M elevated temperature aluminum alloys developed are the Al-Fe-V-Si alloys designed by Allied Signal Inc., which are produced by planar flow casting [5,6]. Alloys are named due to their alloying elements as FVS0812, FVS1212 and FVS0611. FVS0812 and FVS1212 showed very high strengths at 315°C and usable strengths at 425°C. It is reported that the microstructures of these alloys have very finely dispersed silicides that contribute greatly to the strength over a wide temperature range without degrading the corrosion resistance.

FVS0812 alloy is used for aircraft wheels and replaced the 2014 alloy. Moreover, its elevated temperature stability and high strength at temperatures above 300°C makes it challenging to titanium alloys used in some engine components.

Allied Signal Inc. produces the FVS0611 alloy for applications that require good formability, which has a lower alloying element content.

Another elevated temperature aluminum alloy is developed by scientists in Alcan Int. Ltd. They used the Al-Cr-Zr system because of the lower sensitivity to the cooling rate and the better hot workability. It is stated that both chromium and zirconium can produce thermally stable solid solutions even at modest solidification rates. After the consolidation of the powder product, it could be extruded or rolled with low stresses and they aging could be done to obtain stable intermetallics, which give the elevated temperature strength. [7]

Table 2.1 Mechanical properties of elevated temperature aluminum alloys. [1]

Material	Temperature		Yield Strength		Tensile Strength		Elongation %	Fracture Toughness K_{IC}	
	°C	°F	MPa	ksi	MPa	ksi		MPa√m	ksi√in.
Al-8Fe-7Ce	25	77	418.9	60.8	484.9	70.3	7.0	8.5	7.7
	316	600	178.1	25.8	193.8	28.1	7.6	7.9	7.2
Al-8Fe-2Mo-1V	25	77	323.5	46.9	406.6	59.0	6.7	9.0	8.2
	316	600	170.0	24.6	187.5	27.2	7.2	8.1	7.4
Al-10.5Fe-2.5V	25	77	464.1	67.3	524.5	76.1	4.0	5.7	5.2
	316	600	206.3	29.9	240.0	34.8	6.9	8.1	7.4
Al-8Fe-1.4V-1.7Si	25	77	362.5	52.6	418.8	60.7	6.0	36.4	33.1
	316	600	184.4	26.7	193.8	28.1	8.0	14.9	13.6

2.2 Rapidly Solidified Al-Fe-V-Si Alloy

In recent decades there has been a considerable amount of effort devoted to the development of aluminum alloys with high temperature stability which can compete with titanium alloys on a specific strength basis. Al-Fe-V-Si alloys have attracted considerable interest and are widely used in aerospace and automotive industry applications due to excellent room and high temperature strength, thermal stability, fracture toughness and good corrosion resistance [8-10]. These alloys are generally processed through rapid solidification powder metallurgy processing routes due to low diffusivity Fe and V in Al in high cooling rates [12] and it is observed that addition of V to the Al-Fe-Si alloy stabilizes the cubic $Al_{12}(Fe,V)_3Si$ phase over the detrimental Al-Fe intermetallics and also the silicide phase is said to be responsible for the low coarsening rate up to about 773K giving the alloy its high temperature properties[13]. It is also reported that the microstructure Al-Fe-V-Si alloys consist of very fine, nearly spherical $Al_{12}(Fe,V)_3Si$ (silicide) dispersoids, formed from the decomposition of the rapidly solidified microstructures, uniformly distributed throughout the aluminum matrix [14,15]. Moreover, these alloys are devoid of any coarse needle or plate-like intermetallic phases that degrade alloy ductility and fracture toughness [14]. Recently, it is

reported that under normal die casting conditions ten-armed star shaped crystals of Al_3Fe intermetallic phase precipitates [16] and they may act as stress raisers being detrimental to mechanical properties [17]. The Al-Fe-V-Si alloys contain high transition element concentrations (5.5-12.5 wt% Fe) that form high volume fractions of silicides and their desirable microstructural morphology, which can be achievable by rapid solidification techniques, essentially controls the mechanical properties of these alloys.

Table 2.2 Mechanical properties of Al-Fe-V-Si alloy [1].

Test Temperature		Yield Strength		Ultimate Tensile Strength		Elongation	Young's Modulus	
°C	°F	MPa	ksi	MPa	ksi	%	Gpa	10 ⁶ psi
24	75	413	60	462	67	12.9	88.4	12.8
149	300	345	50	379	55	7.2	83.2	12.0
232	450	310	45	338	49	8.2	73.1	10.6
316	600	255	37	276	40	11.9	65.5	9.5
427	800	138	20	155	22	15.1	61.4	8.9

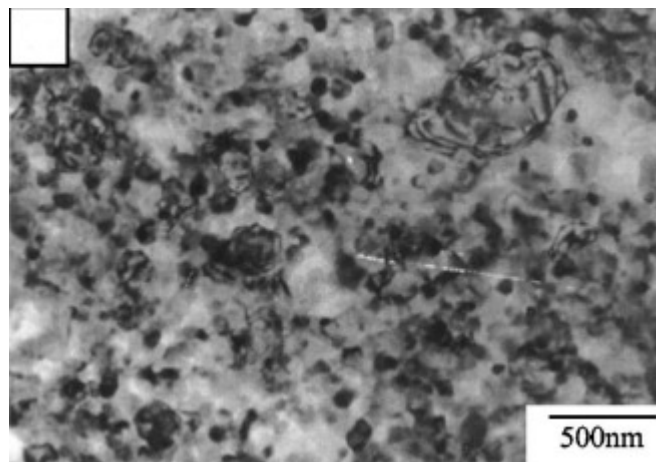


Figure 2.1 TEM micrograph showing the fine dispersed $\text{Al}_{13}(\text{Fe},\text{V})_3\text{Si}$ silicides. [11]

2.3 Spray Deposition

2.3.1. Features and History of Spray Deposition

Although numerous property improvements have been demonstrated to result from rapid solidification, commercialization has been limited due to difficulties associated with the production of bulk shapes. These problems are largely associated with the oxides present on aluminum particulates. In an effort to control the volume fraction of oxides present in consolidated reactive rapidly solidified alloys obtained by powder metallurgy (PM), and to simplify the overall processing, spray atomization and collection processes are being studied in several institutions.

The principles of spray deposition were pioneered during the 1970s by A. Singer at the University College of Swansea, United Kingdom. Singer proposed the production of rolled strip directly from molten metal as an alternative to the current practice of casting and rolling large ingots [18,19] Singer studied the spray rolling of metals as an alternative to a process originally developed at the Reynolds Metal Company in 1967 [20]. In this process aluminum was centrifugally atomized, reheated, fed into roll gaps and hot-rolled to produce strip in a continuous operation [20-22]. The general principle of spray deposition is to atomize a stream of molten metal by means of high velocity gases (i.e., argon or nitrogen) and to direct the resulting spray into or onto a shaped collector (mold or substrate). On impact with the collector the particles flatten and weld together to form a hot, high density preform which can be readily forged to form a fully dense product. The surface of the substrate must be prepared in such a way that the first layer of atomized droplets will adhere to form a smooth quenched layer. Singer conducted most of his work on aluminum alloys. The atomized droplets were approximately 100-150 μm in diameter, and were produced by using conventional atomization equipment. The process parameters used in these studies were sufficient to atomize a melt stream and to cool the particles to temperatures near

the solidus during a flight path of about 18 in (0.45 m). One of the main problems associated with this process of strip making was that the thickness of the as-deposited strip was not uniform across the width [23].

Several years later, Osprey Metals Ltd. (Neath, South Wales) successfully applied the early ideas of Singer for the production of forging preforms. This effort was undertaken as a result of increasing pressures on the metal-forming industry to reduce manufacturing costs, improve material utilization, improve material structure and properties, and increase efficiency [21-28]. The Osprey process became an attractive alternative to the two existing basic methods of producing forgings: (1) the forging route, and (2) the PM method. The conventional forging route employing rolled stock was very inefficient on account of the large quantities of scrap generated. The powder process is relatively expensive as a result of the necessary sieving, reducing, blending, compacting and heating, and due to problems associated with oxide contamination [25].

It would appear that a spray deposition approach will inherently avoid the extreme thermal excursions, with concomitant degradation in mechanical properties and extensive macrosegregation, normally associated with casting processes. Furthermore, this approach also eliminates the need to handle fine reactive particulates, as is necessary with powder metallurgical processes. A series of studies based on the early spray atomization and collection processes, but using high pressure gas atomization for the spraying of fine, rapidly quenched droplets under a tightly controlled atmosphere resulted in the development of other spray deposition processes; these include liquid dynamic compaction (LDC) [29], and variable co-deposition of multiphase materials (VCM) [30].

One particular spray deposition set-up is shown in Figure 2.2.

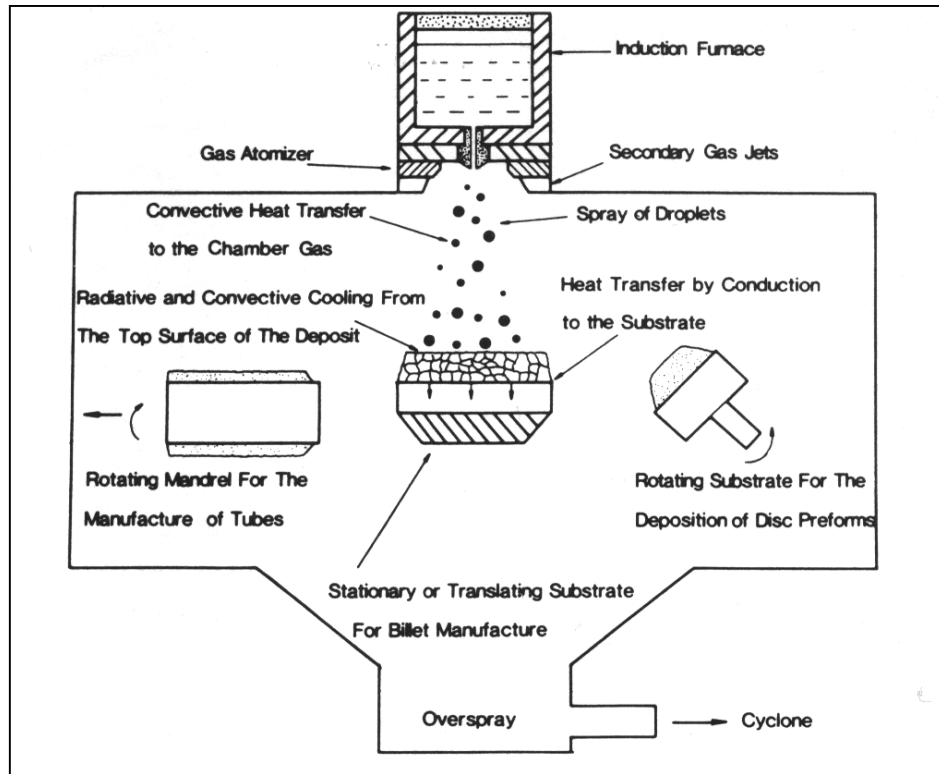


Figure 2.2 Spray deposition set-up [31]

2.3.2 Fundamentals of Spray Deposition

In spray atomization and deposition process, the microstructural characteristics of the spray-deposited material depend to a great extent on the conditions of the droplets prior to impact; that is, on the relative proportions of liquid and solid present, temperature, velocity, and size of the microstructure in both the partially and fully solidified droplets. It is also important to know the size and distribution of the droplets since the amount of heat dissipated by droplets during flight is strongly dependent on their size. The microstructural evolution during spray atomization and deposition can be separated into two distinct but closely related stages. The first stage encompasses those phenomena that are primarily active in the atomized spray prior to impact. The second stage commences after the droplets have impacted the deposition surface, and alteration of the microstructure resulting from impact must be considered.

At the moment of impact, the thermal and solidification conditions of the droplet distribution will depend on;

- (1) the thermodynamic properties of the material,
- (2) the thermodynamic properties of the gas,
- (3) the processing parameters.

The first step towards developing a better understanding of the evolution of the microstructure after deposition and impact, is to establish the thermal conditions of the growing deposit. Recently, various investigators computed the temperature distribution in a growing deposit utilizing a differential thermal energy balance [32]. In addition to unidirectional heat flow, their analysis incorporates the following assumptions; (1) the thermal conditions of the spray during impact can

be approximated utilizing enthalpy considerations, (2) at the preform-substrate interface, conduction of heat is governed by an interface heat transfer coefficient, and (3) during deposition, the top region of the deposit loses heat through the combined effects of convection and radiation.

The thermal history of the material throughout deposition is dictated, in part, by the rate of transfer of thermal energy from the atomized spray into the deposited material. In turn, the rate of transfer of thermal energy from the spray into the deposit is directly related to the average enthalpy content of the spray at the moment of impact. The average enthalpy content of the spray can be estimated from the weighted average of the total heat content of each and every droplet in the spray. Hence, the total enthalpy content can be calculated from [33].

$$H_{spray} = \frac{\sum H_p(di) di^3 f(di)}{\sum di^3 f(di)}$$

where $H_p(di)$ is the enthalpy content of a droplet of diameter di and $f(di)$ is the fraction of droplets with diameter di .

An important microstructural characteristic frequently associated with spray deposited structures is the presence of a finite amount of non-interconnected porosity [30,33,34]. The overall amount of porosity present in spray-deposited materials depends on: (1) the thermodynamic properties of the material, (2) the thermodynamic properties of the gas, and (3) the processing parameters. Under conditions typical for aluminum alloys, the amount of porosity present in spray-deposited materials has been reported to be in the 1-10% range. In addition, the distribution of pore sizes has been shown to be skewed, with a large proportion of pores in the 1-10 μm size range [33,37]. It is interesting to note that several investigators have reported that a large proportion of the fine pores are preferentially located at grain boundaries [30,35,36].

The origin of porosity in spray-deposited materials can be traced to three possible

sources: (1) gas entrapment, (2) solidification shrinkage, and (3) interstitial porosity. The first source, entrapment during impact and solidification, is to be expected as a result of the considerable quantities of gas used to disintegrate the metal during atomization. Recent results, however, suggest that the development of porosity from gas entrapment is not as important a mechanism as originally thought. Ogata et al. [37] reported that the amount of gas contained in a spray-deposited nickel-base superalloy atomized with argon amounted to less than 3 ppm argon. Similarly, fast neutron activation analysis of various spray-atomized aluminum alloys indicated nitrogen levels of approximately 5 ppm [33]. Finally, it is shown that (1) the irregular morphology of the pores, and (2) the limited solubility of the inert gases commonly used for atomization, it is highly improbable that a large proportion of the pores originate from the expansion of entrapped gases [35].

Owing to the limited amount of liquid phase present under proper deposition conditions, it is highly unlikely that solidification shrinkage plays an important role in the formation of the observed pore distribution. Hence, it is anticipated that only under deposition conditions where there is an excessive amount of liquid phase at impact, will this mechanism play a significant role in the formation of porosity. It is important to note, however, that in the presence of excess amounts of liquid phase as a result of: (1) coarse droplet sizes, and/or (2) remelting of solid phases caused by high spray enthalpies, turbulent interactions between the atomizing gas and the molten material will result in the formation of large amounts of porosity. The available experimental evidence suggests that a large proportion of the porosity present develops from interstices formed as the droplets impact on one another, leaving micron-sized, irregular cavities as they overlap. This mechanism is consistent with the observed correlation between deposition conditions such as spray density, powder size, and fraction solidified, and the amount of porosity present throughout the deposit.

An interesting attribute of spray-deposited materials is their microstructural

characteristics. Some investigators [30], studied the microstructure of spray-atomized and deposited Fe-Nd-X materials and reported that although most of structure consisted of equiaxed grains, three types of microstructures could be distinguished: equiaxed grains, 2-20 μm ; solid powders 1-5 μm ; and splats 0.1-1.0 μm in thickness. The presence of these three types of microstructural features was related to the splatting conditions during deposition. At the beginning of the experiment, when spray density as well as the droplet size are largest, it is possible that complete solidification of splats may not occur before the arrival of the next partially solidified or undercooled droplets. Accordingly, a thin film of liquid will be retained on the deposition surface. The mechanical action of the splatting will break off any oxide layer on the droplet surface as well as the delicate dendrite arms in both the depositing droplets and in the liquid film. As a result an equiaxed grain morphology in the microstructure is formed.

To sum up, it can be said that spray deposited materials show characteristic microstructural features as fine equiaxed grained microstructures, absence of metastable phase formation, excess solid solubility, and the absence of macrosegregation.

Finally, to effectively gain advantage of the features of spray deposition explained above, It is reported that, quality and effectiveness of the spray deposition is significantly affected by process parameters so in order to achieve the required deposit shape and desired properties, the following process parameters must be controlled and optimized for the production [38,39,40];

1. The diameter of the melt orifice, hence the melt flow rate,
2. The gas pressure of the atomizer nozzle, hence the gas flow rate,
3. The distance of the substrate from the atomizer nozzle,
4. The inclination of the spray cone due to the substrate,
5. The gas impinging angle,
6. The protrusion length of the nozzle,

7. The shape of the substrate itself,
8. The movement of the substrate.
9. The amount of superheating of the melt.

2.4 Spray Rolling

High strength aluminum alloys are used extensively for aerospace applications. Flat products are manufactured by conventional ingot metallurgical (I/M) processing. Ingots are direct-chill (DC) cast to about 0.6m thickness, scalped, homogenized and hot rolled to the desired thickness. Following this, the material is further processed (e.g. heat treated, cold rolled to final gauge, etc.) according to temper requirements and desired properties. I/M processing remains the most reliable, versatile production method for these alloys. However, it is energy and capital equipment intensive, reflecting the need to homogenize ingots and hot work casting flaws.

Twin-roll casting, was originally proposed by Bessemer in the mid 1800s [41]. It combines solidification and hot rolling in a single operation. Liquid metal is fed into the gap between large water-cooled hollow rolls, where it solidifies to form strip up to about 6mm thick. Since its use began in industry, about 50 years ago, the technology has improved steadily, particularly in the last 20 years. However, twin-roll casters operate much slower than their theoretical production-rate limit to satisfy quality requirements. And, due to production rate and quality issues, commercial sheet has been limited to alloys that have a suitably narrow freezing range [42-47].

At the present time, twin-roll casting is not used commercially to process the 2124 and 7050 alloys. A new strip/sheet casting process, termed “spray rolling” (also “spray strip casting”), is currently under development.[48]. The general concept of spray rolling, i.e., deposition into a roll gap to form strip, is credited to A. Singer

who conducted pioneering work during the 1970s [18]. In general terms, spray rolling combines features of twin-roll casting and spray forming (spray deposition). Spray rolling consists of atomizing molten metal with a high velocity inert gas, extracting most of the metal's latent heat in-flight via convective cooling by entrained inert gas (to about 70% solid), and depositing the atomized droplets between mill rolls. The metal is consolidated into strip/sheet while still in a semi-solid and highly formable condition. As with twin-roll casting, it is believed that some solid state compaction (hot rolling) occurs as the strip advances through the roll gap. While spray rolling shares many similarities with twin-roll strip casting, there are important differences:

1. In twin-roll casting, the metal's superheat and latent heat are dissipated almost exclusively by conductive heat transfer to water-cooled rolls. In spray rolling, convective heat transfer from atomized droplets plays a prominent role and teams with conductive transfer at the rolls to increase production rate.
2. The metal introduced to the rolls in twin-roll casting is molten, while in spray rolling, it has a "slushy" character. Solid particles in the slush act as nucleation sites, producing an equiaxed grain structure and limiting segregation

Aluminum alloys with high solute content and broad freezing ranges have been successfully spray rolled. While still in the early stages of development, spray rolling shows promise for reducing strip/sheet manufacturing costs while improving quality. The inherent rapid solidification and solid solubility extension may, in the future, provide an interesting avenue for the development of alloys tailored for the process and which show unique combinations of properties. Advantages of spray rolling over conventional I/M processing appear to include cost reduction and the elimination of energy intensive unit operations such as ingot casting, homogenization and hot rolling. When compared to twin-roll strip casting, advantages appear to be the high quality and production rate, and the ability to process a broader range of alloys[48].

The spray rolling set-up designed by K.M. McHugh et al. [48] is shown in the Figure 2.3.

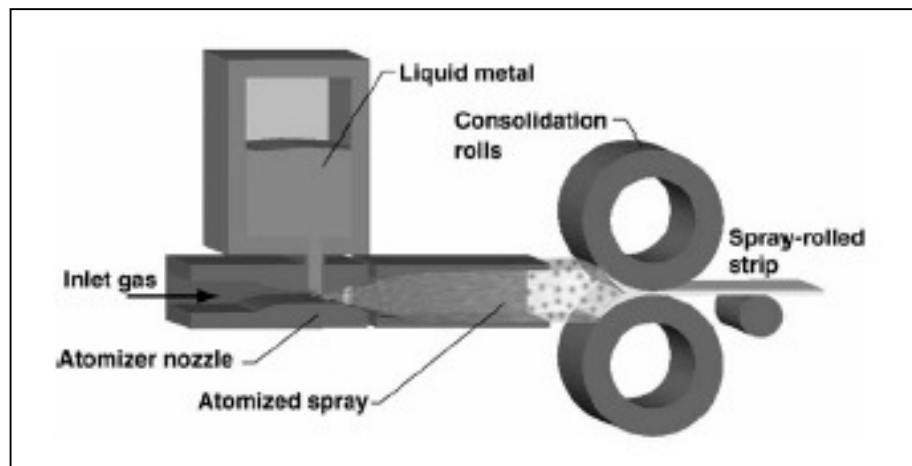


Figure 2.3 Spray rolling set-up designed by McHugh et al.

CHAPTER 3

EXPERIMENTAL PROCEDURE

3.1 Alloy Preparation and Composition

The alloy is melted in inductotherm induction furnace at 800°C and then poured into the furnace of spray rolling set-up, which allows the flow of the alloy melt thorough to the atomizer nozzle.

Two different compositions of Al-Fe-V-Si alloy are used in this study, alloys are prepared from pure Al, pure Fe, ferrovanadium FeV, pure Mg and pure Si. Mg is added to the commercial Al-Fe-V-Si alloy because of its known improvements; including the impeding of the growth of the Al-Fe intermetallics in low cooling rates previously studied by Sahoo et al. [49], decreasing the viscosity of the melt experienced in previous studies and ability to form Mg₂Si resulting in precipitation hardening when heat treatment is conducted.

The alloy compositions are given in Table 3.1

Table 3.1 Table of alloy compositions

	Al(% wt)	Fe (% wt)	V(% wt)	Si(% wt)	Mg(% wt)
Alloy 1	Bal.	8	1.7	8	1.5
Alloy 2	Bal.	8	1.4	1.8	1.3
Alloy 2 has a close composition to the commercial alloy FVS812 without the Mg addition.					

3.2 Spray Rolling Set-up Design

As it was stated before the main aim in this study is achieve the continuous production of the Al-Fe-V-Si alloy strip, which is formed by spray deposition and subsequent rolling. To achieve this, horizontal spray deposition is chosen as the rapid solidification route and a horizontal twin-roller is integrated to the set-up.

In the spray rolling process studied in this study, air atomized molten alloy is directed to the rolls aiming the formation of a semi solid deposit between the rolls and subsequent solidification with simultaneous deformation during the passage through the twin roller. The most critical stage in spray rolling process is presumed to be the spray deposition stage since the control of the spray cone is essential. The important process parameters that guide the design stages is summarized and process variables are classified below.

- The diameter of the melt orifice, hence the melt flow rate;
- The gas pressure of the atomizer nozzle, hence the gas flow rate
- The amount of superheating of the melt
- The distance of the substrate from the atomizer nozzle
- The inclination of the spray cone due to the substrate
- The gas-impinging angle
- The protrusion length of the nozzle
- The shape of the substrate itself
- The movement of the substrate

When considering the above process parameters, the process variables that are used in assessment of spray rolling process in this study are tabulated in Table 3.2

Table 3.2 Process variables and corresponding abbreviations

Process Variables	Corresponding Abbreviation
The diameter of the melt orifice, melt flow	Md
The cross sectional area of melt tip of tundish	Mt
The gas pressure of the atomizer nozzle	Pgas
The distance of the rollers from the atomizer nozzle	d
Inclination of the spray cone due to the roller	i
The protrusion length of the nozzle	Pr
Rolling speed of the twin-roller	Sr
Thickness of roll gap	Gr
Super heating of the alloy melt	Ts
Gas impinging angle	α

3.2.1 Early Spray Rolling Set-ups' Design Stages

In order to achieve the continuous production of the flat product several spray rolling set-ups are prepared and experiments are conducted. In the first three newly designed set-up continuous production of the alloy strip can not be achieved but valuable practical information related to the spray rolling process and effects of process parameters is gained.

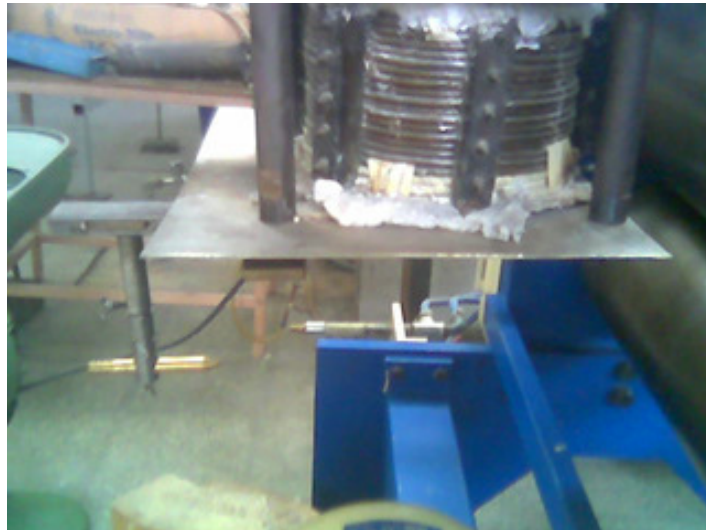


Figure 3.1 First experimental spray rolling set-up

In the first experimental set-up, atomization of the molten alloy is done by a horizontal gas jet focused on the stream of molten alloy, which is allowed to flow vertically from the bottom of the induction furnace. The metal is melted in a separate induction furnace and then poured into the set-up furnace at 800°C. The design parameters “i, Pr and d” are adjustable by the movable gas jet nozzle. The atomizer to roller distance “d” is 50 cm. The protrusion length “Pr” is 20cm. In this set-up continuous atomization of the molten metal cannot be achieved. After the first experiment it is decided to decrease the roller to atomizer distance “d” and the need of a new atomizing nozzle is observed. The photograph and simple sketch of the set-up is shown in Figure 3.1 and Figure 3.4.a respectively.



Figure 3.2 Second experimental spray rolling set-up.

In the second experimental set-up, a new atomizer nozzle is used. The nozzle has a protrusion length “Pr” of 0 cm, gas impinging angle “ α ” of 15° , melt orifice diameter of 12mm. The sketch of atomizer nozzle is shown in Figure 3.3. The atomizer nozzle to roller distance “d” is 10cm. The molten metal is carried from the furnace to the nozzle with the help of a heat resistant tube made of alumina fiber. The photograph and sketch of the setup are shown in Figure 3.2 and Figure 3.4.b. respectively.

The continuous atomization cannot be achieved; main problem observed in this set-up is the early solidification of the molten alloy inside of the heat resistant tube therefore a heat insulation box is integrated to the set-up to decrease the heat loss from the tube. Heat insulation box is made from firebricks fixed inside a metal box.

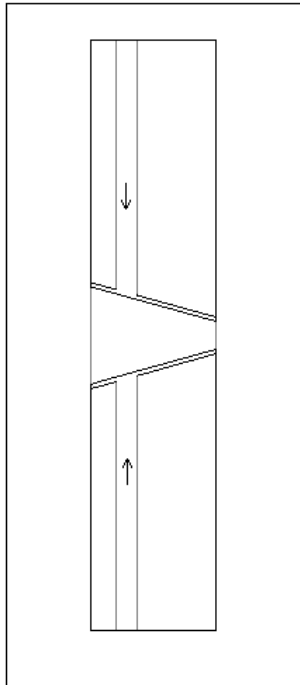


Figure 3.3 Sketch of Atomizer Nozzle

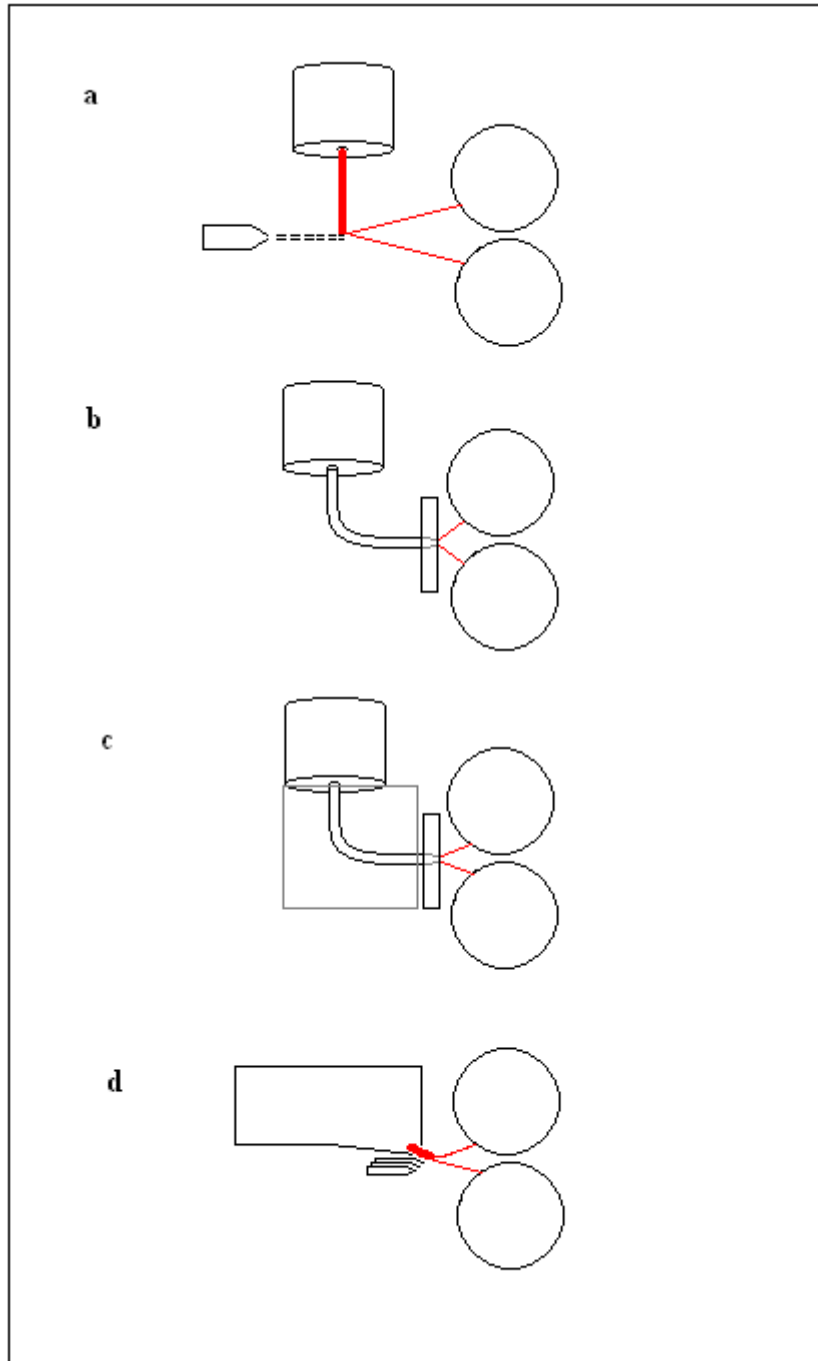


Figure 3.4 Sketches of experimental set-ups

In the third experimental set-up, the heat insulation box that is integrated to the system, retarded the solidification of the molten metal in the tube. Atomization of the molten alloy is taken place but it is observed to be inhomogeneous therefore continuous atomization of the molten alloy is not achieved. The atomizer used in this set-up produces a high angle spray cone, which result in wide spreading of the semi solid powders, which is not appropriate for spray deposition through the roller where a lower angle cone is needed for directing onto the rollers. The heat insulation box is also decided to be insufficient which cannot avoid the heat loss from the system successfully. The sketch and photograph of the set-up with the insulation box is shown in Figure 3.4.c. and Figure 3.5 respectively.



Figure 3.5 Third experimental spray rolling set-up.

3.2.2 Advanced Design of Spray Rolling Set-up

When the results of previous three set-ups are assessed; it is decided that one of the critical process parameter is the superheat of the alloy melt. Although the alloy is poured at 800°C, the temperature of the alloy melt near to the nozzle is significantly lower than that as a result the superheat of the alloy is completely lost. Other critical process parameters are related to the nozzle. The new nozzle design should accomplish the controlled directing of the alloy melt in the semi solid powder form and they should hit the rollers just before solidification. It is concluded that an advanced set-up design concerning the above conclusions is needed.

First design rationale is the loss of the superheat of the alloy melt which can be solved by providing external heat to the system and by supporting the molten alloy front by a heat mass. In order to achieve these goals and electrical resistance furnace is designed and produced. The electrical furnace includes a tundish unit having a reservoir capable of keeping 5 liters of molten alloy.

The electrical furnace is designed to reach a temperature of 1000°C and to be able to keep the molten Al-Fe-V-Si alloy at 800°C - 850°C.

Production of the Electrical Resistance Furnace

The first concern in the furnace design was the insulation of the furnace. For the insulation 50mm. thick alumina fiber block insulators are used. The block insulators are designed to withstand 1500°C. A closed box is formed from the block insulators and then block insulators are carved for the reinforcement of the electrical resistance wire.

For resistance heating, 4 meters of coiled resistance wire is needed to be reinforced inside of the 4 insulator blocks surrounding the furnace. 20 meters of Nickel-Chromium 80-20 resistance wire having a diameter of 1.6mm is used, which has a maximum operating temperature of 1100°C. The resistance wire is coiled into a outer diameter of 9 mm. The coiled wire is stretched with a ratio of 3:1 as a result 4 meters of coiled electrical resistance wire is obtained.

The electrical resistivity of the 80-20 Nickel-Chromium wire is 108μohm.cm. The linear resistance of the wire is calculated below;

$$\begin{aligned} R \text{ (ohm/m)} &= \text{Resistivity } (\mu\text{ohm-cm}) / A \text{ (in mm}^2\text{)} \times 100 \\ &= 108\mu\text{ohm.cm} / 2,0106\text{mm}^2 \times 100 \\ R &= 0,537 \text{ ohm/m} \end{aligned}$$

For 20m. wire total resistance is 10,74 ohm.

From the experimental observations it is known that the variac unit that is connected to the furnace can provide 18amperes of current to the 4 m. coiled wire.

Thus the power of the electrical furnace can be calculated as;

$$\begin{aligned} P &= I^2 \times R \\ &= (18 \text{ amperes})^2 \times 10,74 \text{ ohms} \\ &= 3479,76 \text{ W } 3,4796 \text{ kW} \end{aligned}$$

The photographs of the production of the electrical furnace is shown in Figure 3.6



Figure 3.6 Photographs of electrical resistance furnace production.

As a result of electrical resistance furnace production the problem of insufficient superheat of alloy melt is solved and continuous flow of the alloy melt is achieved. The next design parameter mainly concerned is the nozzle design. In the new set-up a flat horizontal gas nozzle is used for atomization, which is 25mm wide and has a inner thickness of 1mm. In the new set-up most of the critical process parameters can be controlled, using the advanced set-up numerous experiments are conducted with changing the process variables. Last three set-ups are classified as Stage 1, Stage 2 and Stage 3 having a positive evolution in the achievement of the continuous flat product.



Figure 3.7 Advanced experimental spray rolling set-up

In design stage 1, electrical resistance furnace is heated up to 800°C. The details of the process variables are given Table 3.3. After the molten metal that is melted in the induction furnace is poured into tundish atomization of the melt is begun, as a result of the large tundish tip the melt flow rate was too high and the atomization of the melt resulted a flow of semi solid particles rather than semi solid powders. Powder sized atomization is achieved near the end of batch, while the spray deposition is taking place it is observed that a significantly large spray cone is formed and as a result spray deposition has taken place in a wide area over the rollers so solidification between the roll gap cannot be achieved. After the experiment it is decided to decrease the roller to atomizer distance to obtain a smaller spray cone, to decrease the melt flow rate to obtain finer atomization.

In the design stage 2, electrical resistance furnace is heated up to 850°C to obtain a better super heating of the alloy since the metal flow rate is decreased. After the atomization is started, it is observed that the solidification between the roll gap is succeeded and spray rolled products are obtained. However, the production is not continuous short strips are formed. Subsequent to formation in the roller one set of strips allowed to cool in water and the others allowed cooling in air. It is decided that the roller speed should be decreased and the melt flow rate should be decreased to have better spray deposition over the rollers and better solidification in the roll gap. Details of process variables is shown in Table 3.3

In the design stage 3, the electrical resistance furnace is heated up to 850°C. A new composition of Al-Fe-V-Si alloy having lower Si content is used. As a result of decreased roller speed and homogeneous spray deposition achieved by the decreased molten metal flow rate, formation of continuous flat product of Al-Fe-V-Si alloy is achieved. Details of process variables is shown in Table 3.3 The photograph of flat Al-Fe-V-Si alloy is shown in Figure 3.8

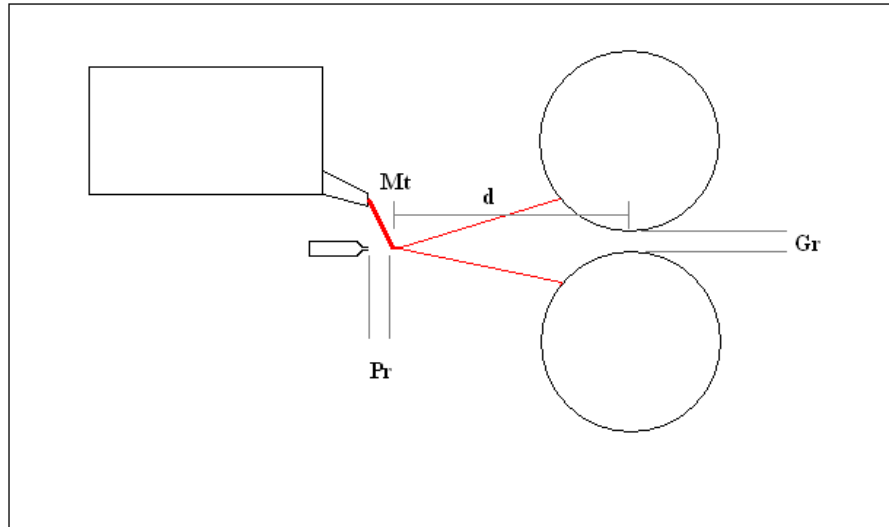


Figure 3.8 Sketch showing the process variables

Table 3.3 Detailed tabulation of process variables in the related design stages

Process Variables & Abbreviation		Design Stage 1	Design Stage 2	Design Stage 3
The cross sectional area of melt tip of tundish	Mt	30mm x 15mm	20mm x 10mm	10 mm x 5mm
The gas pressure of the atomizer nozzle	P _{gas}	98.06 kPa	196.13 kPa	196.13kPa
The distance of the rollers from the atomizer nozzle	d	400mm	300mm	300mm
The protrusion length of the nozzle	Pr	20mm	10mm	10mm
Rolling speed of the twin-roller	Sr	92.3 mm/s	103.3 mm/s	67.0 mm/s
Thickness of roll gap	Gr	2mm 3mm end product	2mm 3mm end product	2mm 3mm end product
Super heating of the alloy melt	Ts	Furnace kept at 800°C	Furnace kept at 850°C	Furnace kept at 850°C
Gas impinging angle	α	0°	0°	0°



Figure 3. 9 The continuous flat Al-Fe-V-Si alloy product



Figure 3. 10 Photograph of spray rolling process

3.3 Hot Rolling

Hot rolling of the specimens is made in the same twin roller that is used in the spray-rolling set-up. The specimens are heated up to 450°C in the electrical resistance furnace and kept for 120 min. before rolling. Hot rolling resulted a %20 reduction in the thickness of the specimen.

3.4 X-Ray Diffraction Study

X-ray diffraction study is made for characterization of phases present in the spray rolled products. The study is performed by Rigaku International Company D/MAX2200/PC ULTIMA X-ray Diffractometer by CuK α radiation having λ :1.5409.

3.5 Optical and Scanning Electron Microscopy Study

Optical and Scanning Electron Microscopy is carried out to examine the microstructural features of the spray rolled products. The equipment used for SEM is a JSM-6400 Electron Microscope (JEOL) equipped with NORAN Series II Microanalyzer System. This microscope is capable of having secondary and backscattered electron images and EDX microanalysis.

Etching of the Al-Fe-V-Si alloy specimens is done by the Kellers reagent.

3.6 Hardness Test

Brinell hardness (HB) values are obtained by using Heckert hardness testing machine. Eight data is taken from each specimen aiming the assessment of hardness distribution and calculation of the average hardness.

Hardness covers several properties as resistance to deformation, resistance to friction and abrasion. The following correlation links brinell hardness with tensile strength, while resistance to deformation is dependent on modulus of elasticity.

Tensile Strength (MPa) = $3.55 \times \text{HB}$ (for $\text{HB} < 175$); $3.38 \times \text{HB}$ (for $\text{HB} > 175$)

3.7 Three Point Bending Test

Three point bending test is done with Shimatsu 10kN testing machine from which the Force(N) vs Stroke(mm) data is obtained and then Flexural Stress vs Strain graphs are drawn by the use of following formulations. The maximum flexural stress values calculated by 0.2% offset method since the bending theory is applicable only for elastic deformation.

Bending test specimens have span length of 35mm, width of 10mm and thickness of 3.0mm.

Stress $\sigma = M \cdot c / I$ where $c = t/2$, $M = P \cdot L / 4$ and $I = w \cdot t^3 / 12$

Strain $\epsilon = 12 \cdot y \cdot c / L^2$ where $c = t/2$

P: Load applied by the testing machine,

t: Thickness of the specimen

w: Width of the specimen, and

L: Span length respectively

y: Deflection, stroke applied by the machine.

3.8 Tensile Test

Tensile test is done with Shimatsu 10kN testing machine from which the Force(N) vs Stroke(mm) data is obtained and then Stress (MPa) vs Strain graphs are drawn and tensile strength and % elongation values are determined.

Tensile test specimens have 8.5mm gauge width and 20mm gauge length with thickness values of 3.0mm and 2.4mm(hot rolled).

3.9 True Density Measurement Study

True density measurements of the specimens are made by the Ultrapycnometer1000 Quantachrome Corp., Helium Pycnometer device in the Central Laboratory of METU.

Conclusions concerning porosity are derived by comparing the measured true density of the specimens from different processing conditions.

CHAPTER 4

RESULTS AND DISCUSSIONS

4.1 Phase Characterization

It is known that the process parameters in production significantly affect the microstructural and mechanical features of the final product. Since the primary concern of this study is to design a spray rolling process, the microstructural and mechanical property results obtained in each process development stage is used for further design concerns.

Phase characterization study is made to investigate the morphology, existence and distribution of both expected and unexpected intermetallic and silicide phases in the spray rolled Al-Fe-V-Si alloy. In order to access the results clearly metallographic and X-ray specimens are classified due to the processing type and stage, which is shown in Table 4.1

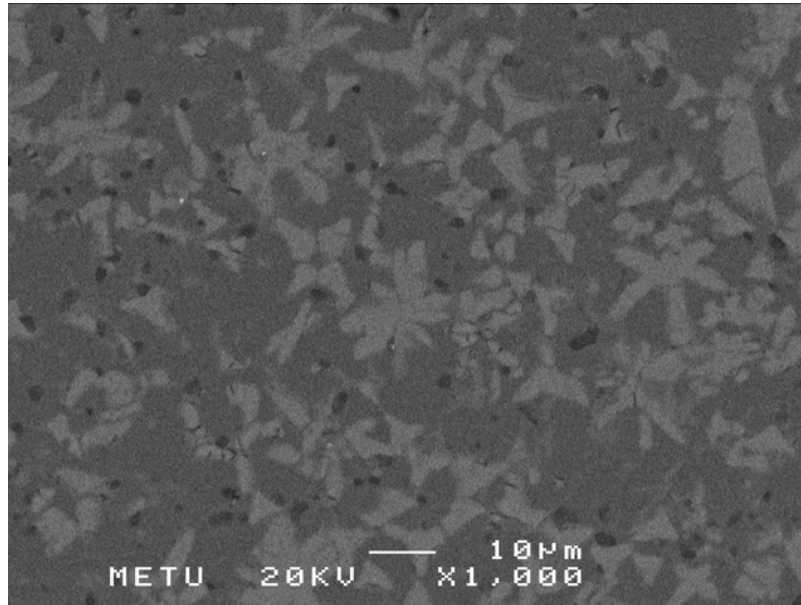
Table 4.1 X-ray and metallographic specimen classification.

Specimen Code	Alloy Comp. *	Set-Up Design Stage *	Further Processing
A1	Al-8Fe-2V-8Si	1	Rolled
A2	Al-8Fe-2V-8Si	2	Water Cooled
A3	Al-8Fe-2V-8Si	2	Air Cooled
B1	Al-8Fe-1V-2Si	3	Water Cooled
B2	Al-8Fe-1V-2Si	3	Air Cooled
B3	Al-8Fe-1V-2Si	3	Hot Rolled

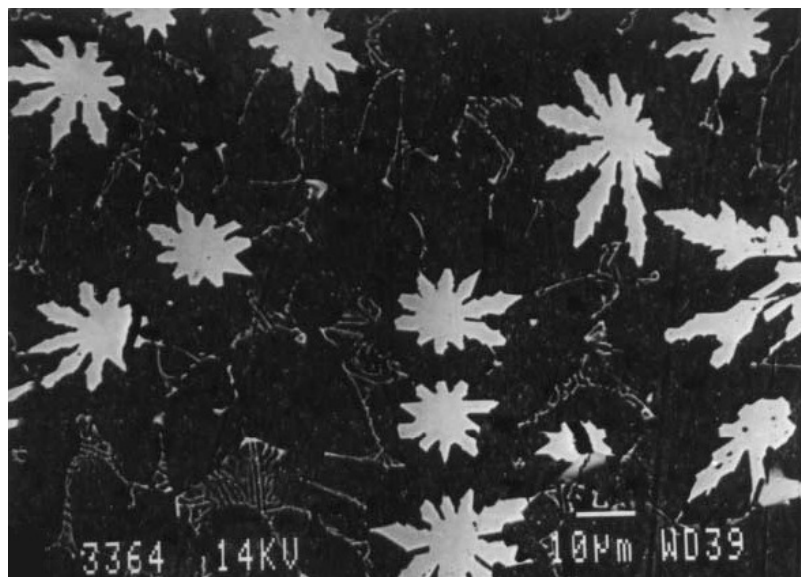
* 1.5%wt Mg is added to all alloys. Design stages are explained in detail at Chapter 2.

4.1.1 Optical and Scanning Electron Microscopy Results

The microstructure of A1 specimen, which is spray deposited and then rolled in as cast condition features; high level of porosity and starlike precipitates, formerly characterized as Al_3Fe and $Al_{13}Fe_4$ by Sahoo et al. [16,49], which are finer than the conventionally cast intermetallics, can be shown in Figure 4.1. Moreover, band shaped rodlike intermetallic phases are observed in a separate area, which is evident to the inhomogeneous cooling in the preform. These intermetallic phases are characterized as $Al_{13}Fe_4$ by X-ray diffraction, and in agreement with the characterized phases in the previous study by Kalkanli et al. [50] shown in Figure 4.2. It is stated that in spray deposition of Al-Fe-V-Si alloy growth of these intermetallics are impeded as a result of high cooling rate [50] therefore one can conclude that the cooling rate achieved in the present setup is not adequate. An intermetallic phase that is observed is characterized as V_3Si by X-ray diffraction, is unevenly distributed over the $Al_{13}Fe_4$ intermetallics, probably formed as a result of high Si content in the alloy. EDX analysis is shown in Figure 4.3 and SEM and optical micrograph is shown in Figure 4.4.



(a)



(b)

Figure 4.1 Starlike intermetallics (a) in specimen A1 (b) from Sahoo et al. [10]

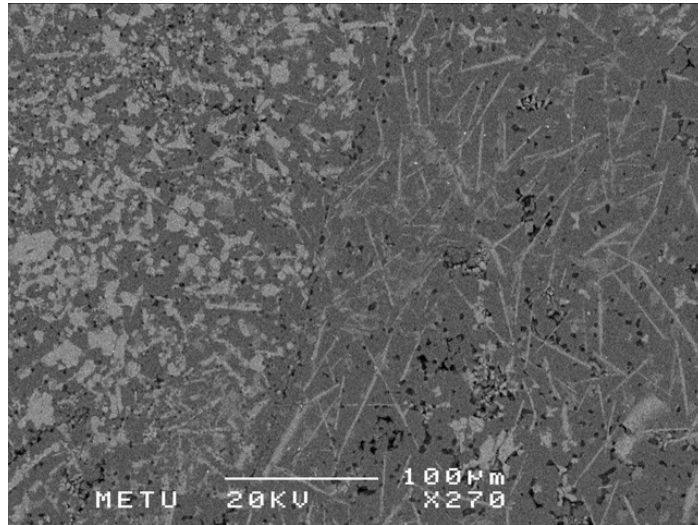
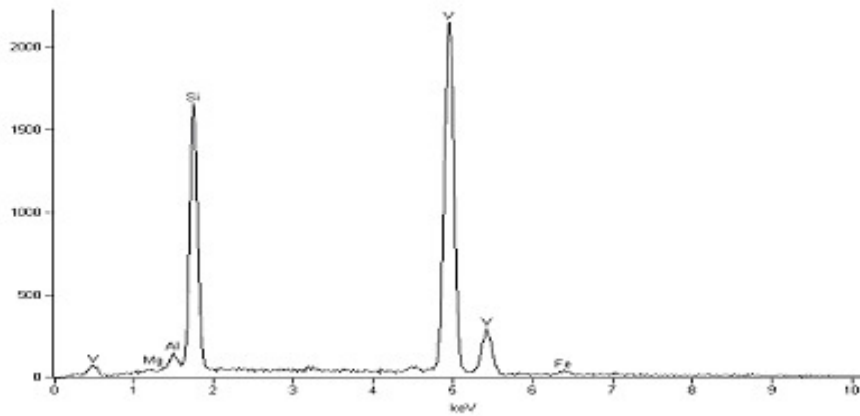
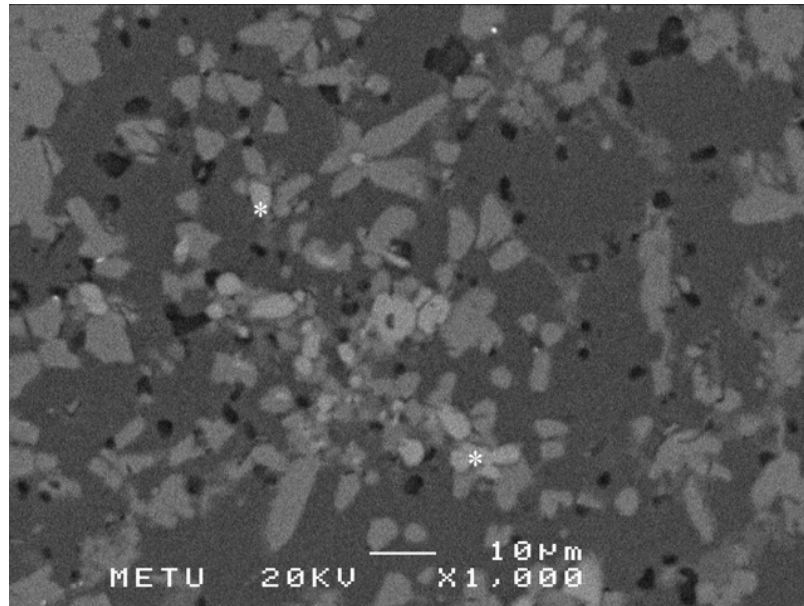


Figure 4.2 Inhomogeneous area featuring $\text{Al}_{13}\text{Fe}_4$ intermetallics.

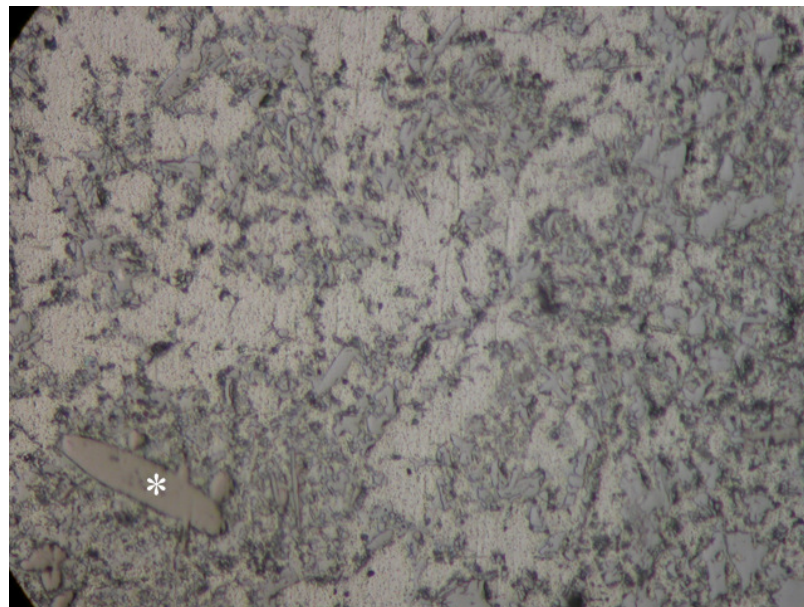


<i>Element</i>	<i>Weight Conc %</i>	<i>Atom Conc %</i>
Mg	0.03	0.05
Al	1.52	2.38
Si	23.36	35.23
V	73.74	61.31
Fe	1.35	1.03

Figure 4.3 EDX analysis of V_3Si intermetallic.



(a)

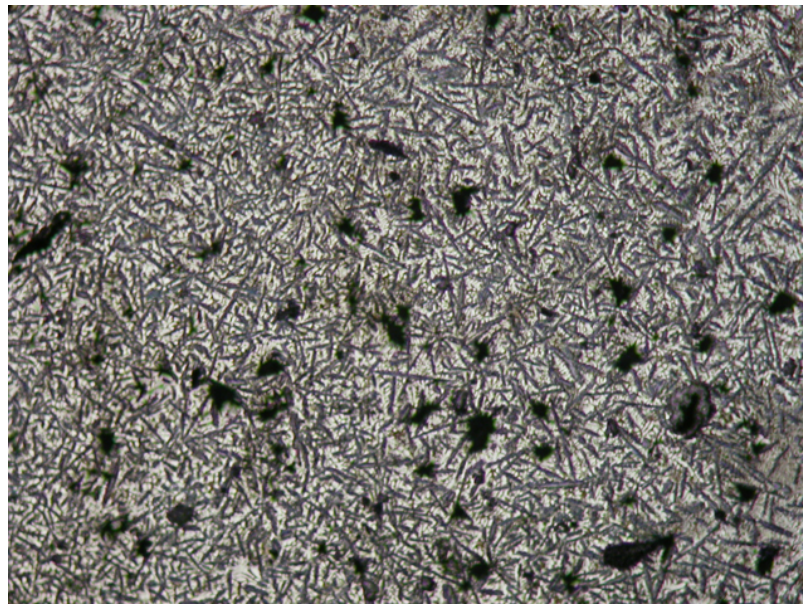


(b)

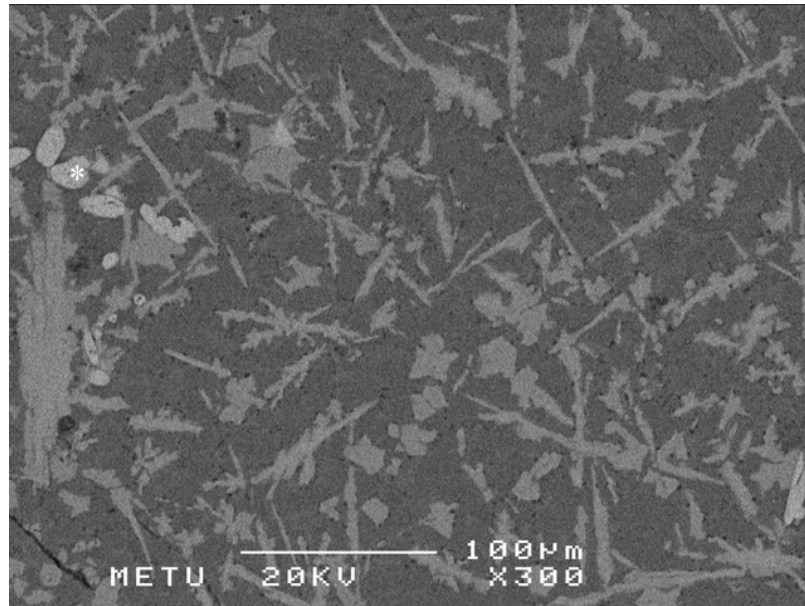
Figure 4.4 V₃Si intermetallic phase marked by * (a) SEM micrograph in X1000 magnification, (b) optical micrograph in X500 magnification.

The specimen A2 is formed in the second design stage of the set-up, which features smaller tundish opening to decrease molten metal flow aiming to achieve finer atomization of the stream. In addition to this a water tank is integrated to the system in order to achieve a higher cooling rate in the as formed metal strip.

The microstructure of the A2 specimen is finer than A1 due to the better atomization achieved by decreasing the molten metal stream. Large amount of porosity is observed in the specimen and the phases present are characterized as band shaped rod like $Al_{13}Fe_4$ intermetallics distributed densely through the matrix and V_3Si intermetallics distributed unevenly through the matrix. No starlike intermetallics are observed probably the growth is avoided due to the cooling rate achieved during the atomization. The growth of $Al_{13}Fe_4$ intermetallics into band shaped morphology is a result of inadequate cooling rate. Although water-cooling is expected to introduce a higher cooling rate, the amount of water is not enough to cool the as cast preform it rather be heated up and resulted in an inadequate cooling rate. Optical and SEM micrographs and EDX analysis of A2 is shown in Figure 4.5 and Figure 4.6.



(a)



(b)

Figure 4.5 (a) optical micrograph of A2 in X50 magnification, (b) SEM micrograph showing $\text{Al}_{13}\text{Fe}_4$ and V_3Si (*) intermetallics in X300 magnification.

<i>Element</i>	<i>Weight Conc %</i>	<i>Atom Conc %</i>
<i>Mg</i>	0.04	0.07
<i>Al</i>	0.88	1.38
<i>Si</i>	23.98	36.17
<i>V</i>	74.31	61.79
<i>Fe</i>	0.79	0.60

Figure 4.6 EDX analysis of V_3Si intermetallic in specimen A2.

Specimen A3 is produced by the same tundish and that is used with A2, only difference is A3 is cooled in air after spray rolled into a strip. Microstructure of A3 features homogeneous distribution of rounded intermetallics having an average diameter of 10 μ m. There is also band shaped Al₁₃Fe₄ intermetallics but they are observed as cracked. Moreover, V₃Si intermetallic phase is observed in the specimen, which expected due to the high Si content in the alloy composition.

Optical micrographs of specimen A3 showing fine rounded Al₁₃Fe₄ intermetallics is given in Figure 4.7, and SEM micrograph showing round intermetallics, V₃Si intermetallic and cracked band shaped intermetallic is given in Figure 4.8.

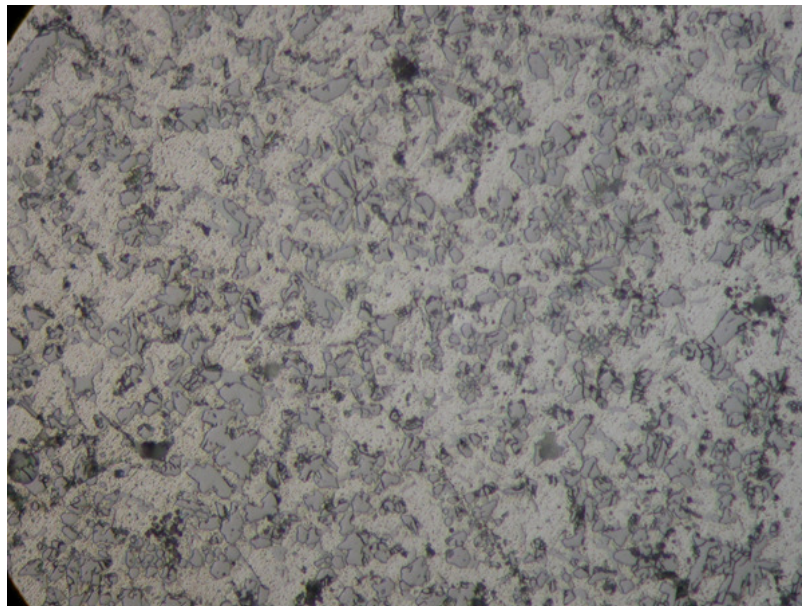
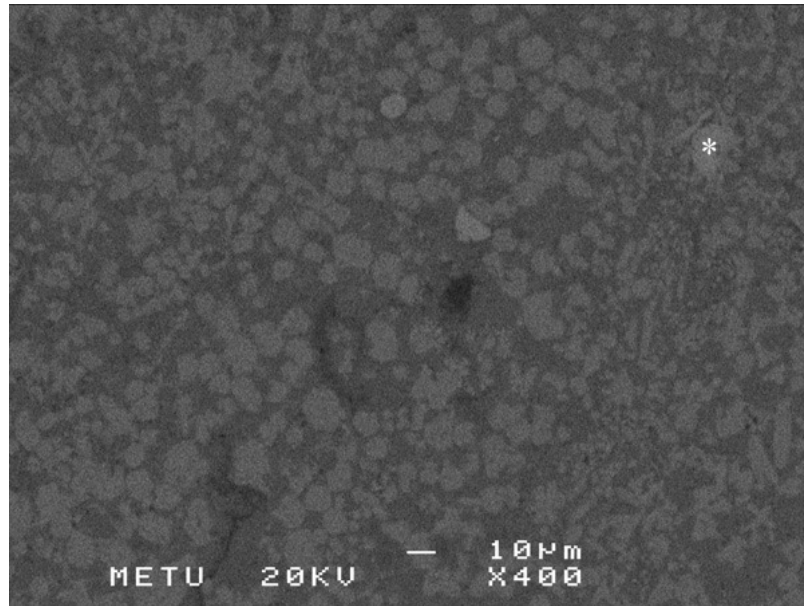
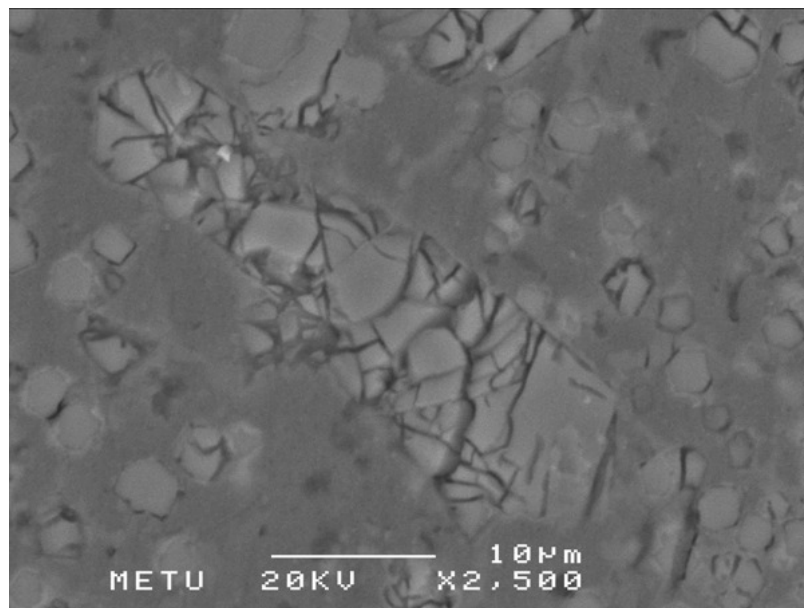


Figure 4.7 Optical Micrograph of A3 showing fine rounded Al₁₃Fe₄ intermetallics in X500 magnification.



(a)

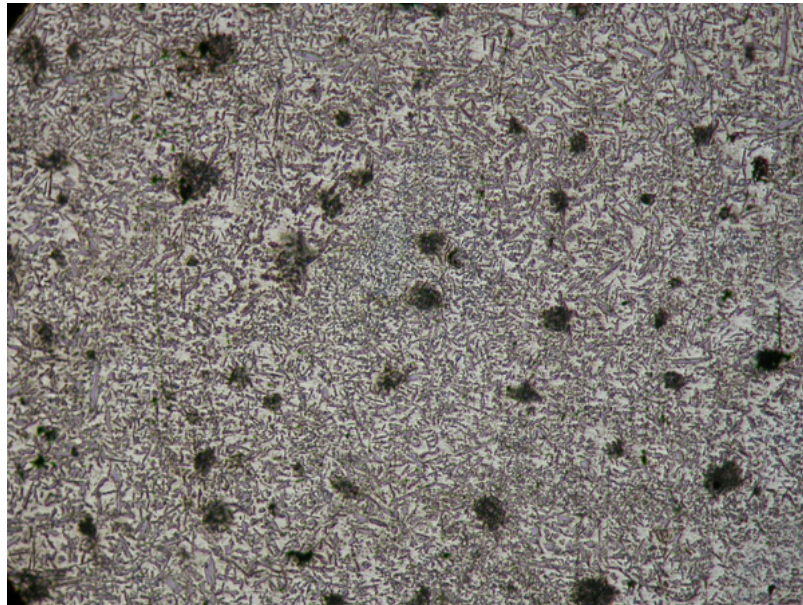


(b)

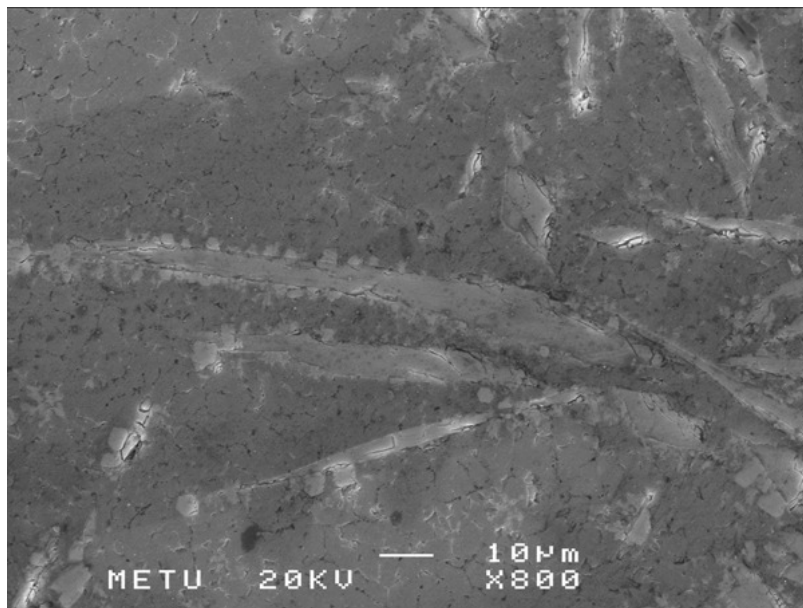
Figure 4.8 SEM Micrograph of A3 showing (a) fine rounded Al-Fe intermetallics and V_3Si (*) in X400 magnification, (b) cracked Al-Fe intermetallic in X2500 magnification.

Specimen B1 and B2 is produced in the third design stage set-up, which features a smaller spraying distance and smaller tundish tip opening so that the air atomization of the alloy and simultaneously rolling of the semi-solid deposit is achieved, resulting a continuous flat Al-Fe-V-Si alloy product. In addition to this, Si content in the alloy is decreased hence changing the alloy composition to Al-8Fe-1.4V-1.8Si + 1.3Mg in %wt.

Specimen B1 is allowed to cool in water after spray rolling and heating up of the water similar to the case in A2 is observed. In the microstructure of B1 band shaped $\text{Al}_{13}\text{Fe}_4$ intermetallics are observed, they are homogeneously distributed in the matrix and finer when compared to the A2, One can conclude that the finer microstructure obtained is a result of successful atomization of the melt and growth of intermetallics to band shape is resulted from the slower cooling rate during the solidification of the strip. The poor water-cooling is suspected to be related to the low amount of water used. Since it is seen that adequate cooling rates can be achieved in air-cooling, instead of using a higher amount of water air-cooling is chosen for cooling of the spray rolled preform. Optical and SEM micrographs of B1 are shown in Figure 4.9, 4.10.



(a)



(b)

Figure 4.9 (a) Optical micrograph of B1 showing fine intermetallics in X50 magnification. (b) SEM micrograph of B1 showing $\text{Al}_{13}\text{Fe}_4$ intermetallic phase.

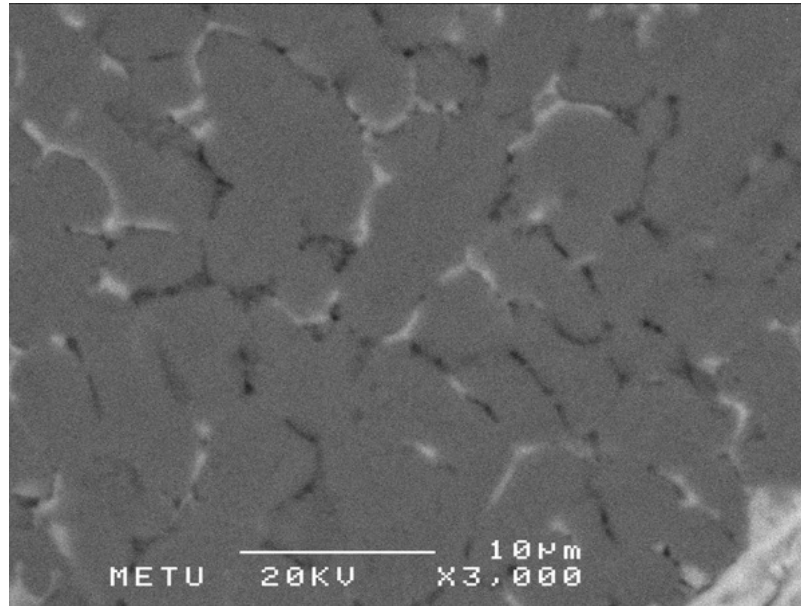
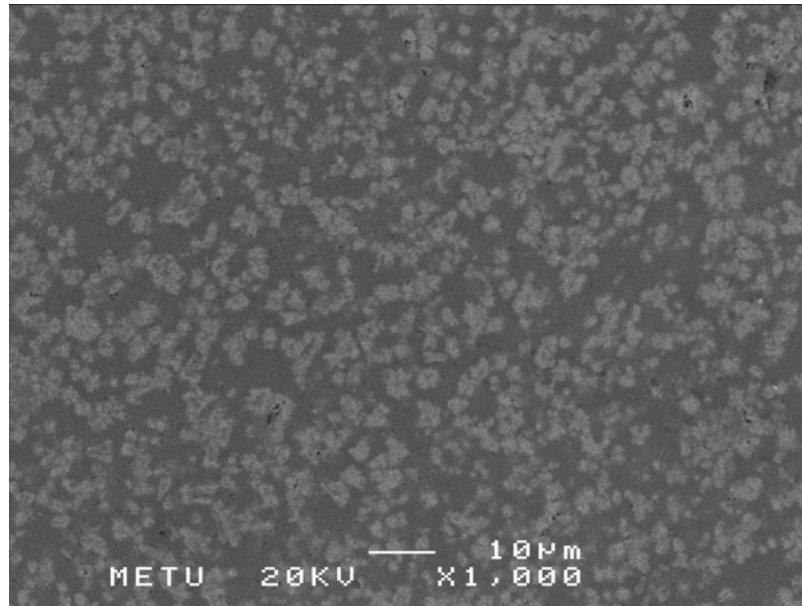
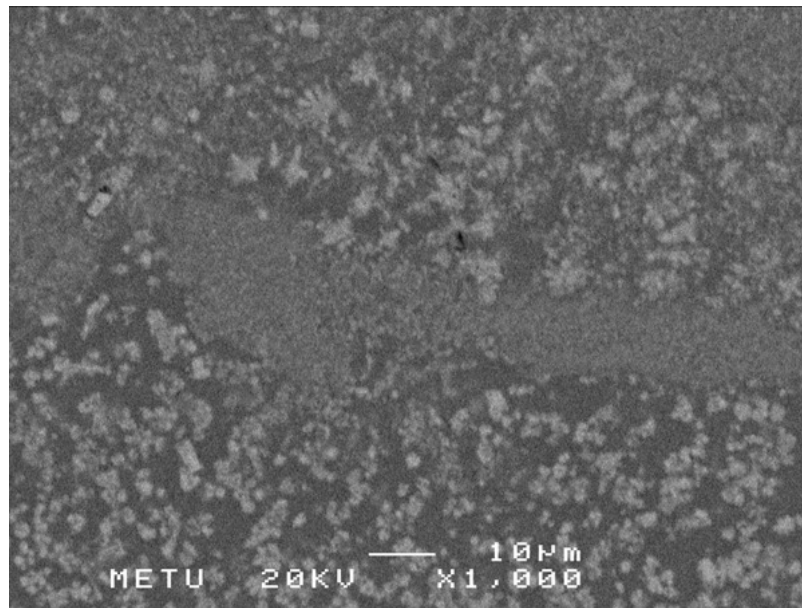


Figure 4.10 SEM micrograph of B1 showing the fine dendrite structure

Specimen B2 is produced in the same set-up as B1 so that successful atomization and the continuous production of the flat product is achieved, moreover B2 is cooled in air after spray rolling. Microstructure of B2 features fine grains and fine rounded Al-Fe intermetallics having an average diameter of 3 - 5 μ m. In addition an Aluminum rich zone is observed in B2 specimen where there is slight amount of intermetallics. Kalkanli et al reported a similar zone in previous study, it is told that Aluminum rich zone is formed during spray deposition as a result of transient liquid formation and segregation of Fe, V and Si atoms during solute rejection from that zone [50]. The intermetallic rich regions around the Al rich zone is in agreement with previous study and probably formed by segregation of solute atoms. Optical and SEM micrographs of B2 are shown in Figure 4.11, 4.12.

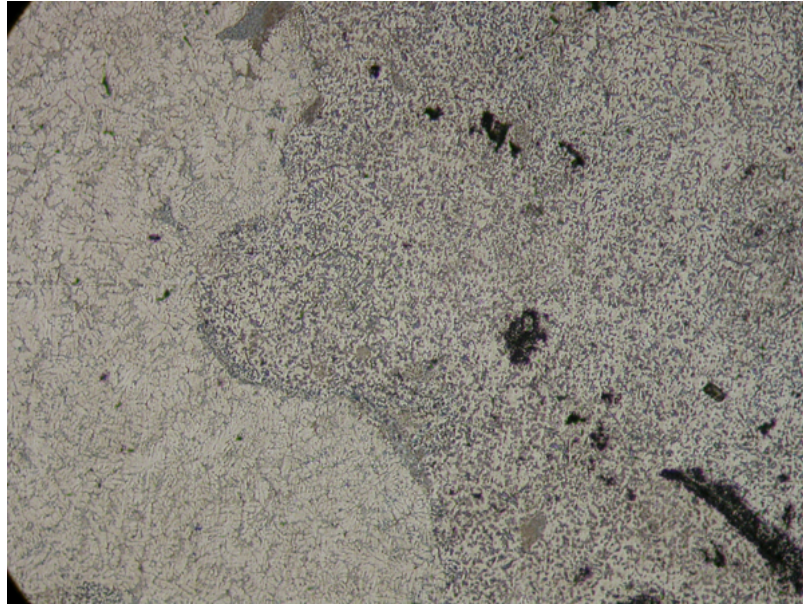


(a)

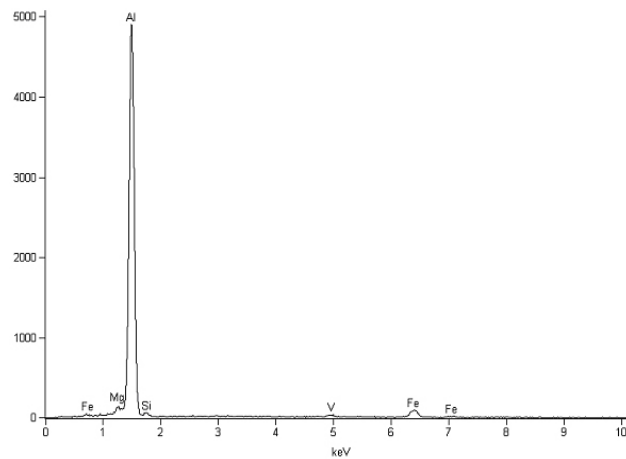


(b)

Figure 4.11 (a) SEM micrograph of B2 showing fine rounded Al-Fe intermetallics in X1000 mag. (b) showing segregation zone in X1000 magnification.



(a)



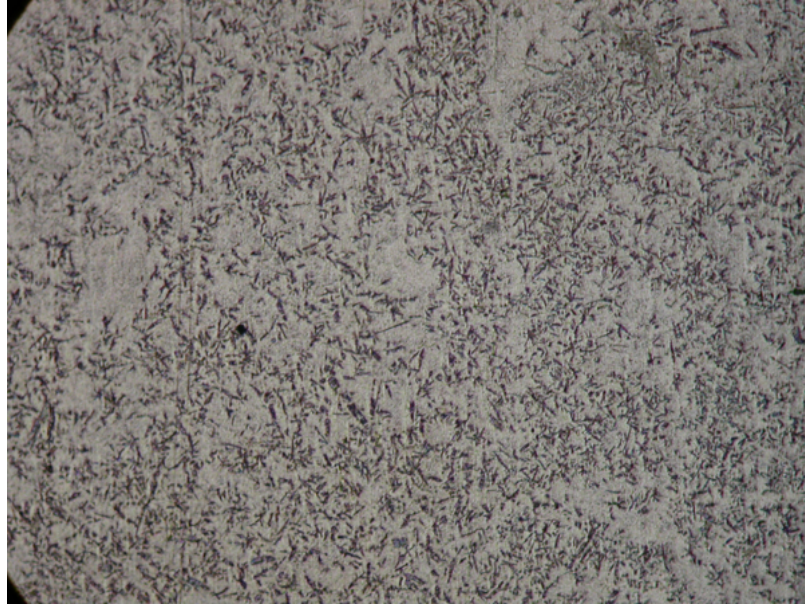
	<i>Conc %</i>	<i>Conc %</i>
<i>Mg</i>	0.60	0.69
<i>Al</i>	88.87	92.91
<i>Si</i>	1.99	2.00
<i>V</i>	1.54	0.85
<i>Fe</i>	7.00	3.54

(b)

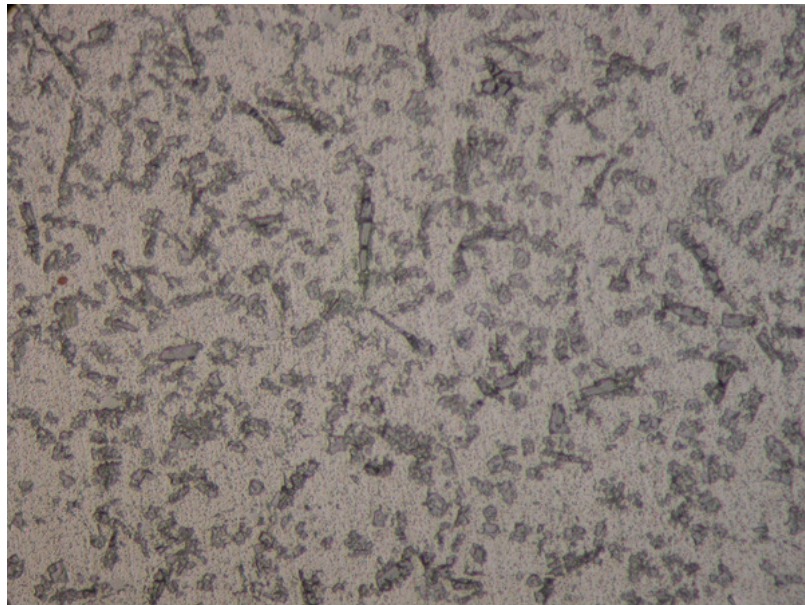
Figure 4.12 (a) Optical micrograph of B2 showing the Al rich segregation zone in X100 magnification. (b) EDX analysis taken from the Al rich zone

Specimen B3 is produced in the same set-up as B2. For the further processing of B3 specimen a hot rolling stage is introduced, aiming the consolidation of the flat product, which contains considerable amount of porosity. Prior to hot rolling specimen is kept at 450°C for 120mins, since the alloy contains Magnesium precipitation of Mg_2Si is considered. In the SEM micrographs of B3 very fine white particles are observed, EDX analysis taken from these particles show the presence of Mg together with the other alloying elements (Fe, V, Si). These particles are presumed to be Mg_2Si precipitates or $Al_{13}(Fe, V)_3Si$ silicides, for the clear characterization of these particles a transmission electron microscopy study is needed since the particles are much smaller than 1 μm .

Microstructure of B3 features both rounded and band shaped intermetallics and they are observed as very fine and homogeneously distributed through the matrix, band shaped $Al_{13}Fe_4$ intermetallics are cracked, porosity level is decreased considerably only microporosity is observed. SEM and optical micrographs of B3 are shown in Figure 4.12 and 4.13.

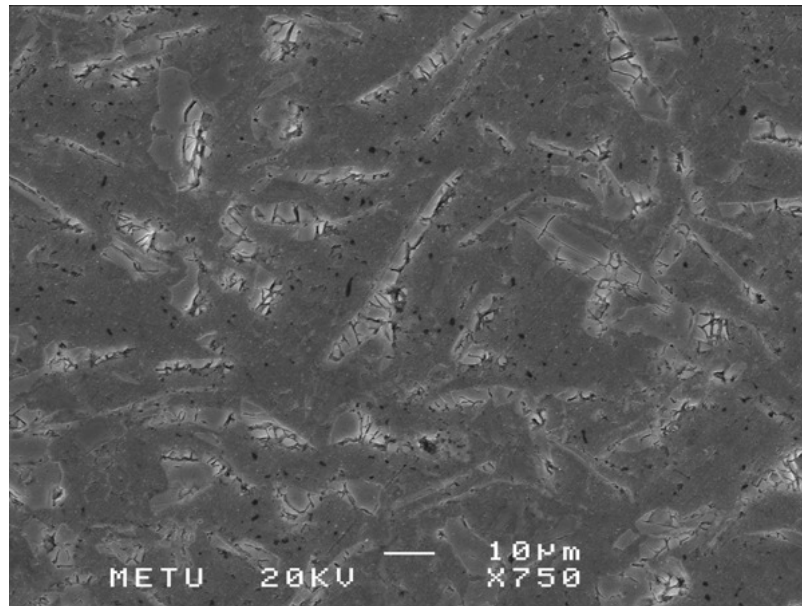


(a)

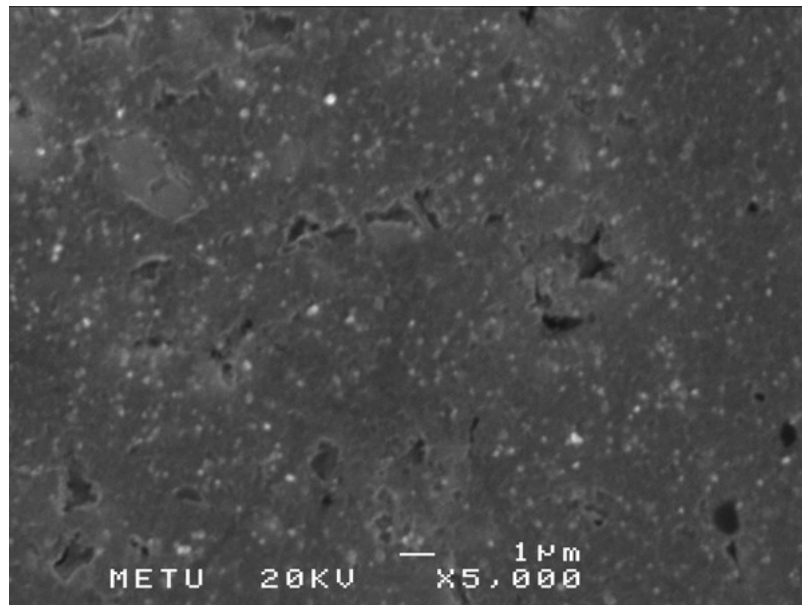


(b)

Figure 4.12 Optical micrographs of B3 showing the homogeneous distribution of intermetallics (a) in X50 (b) X500 magnification.



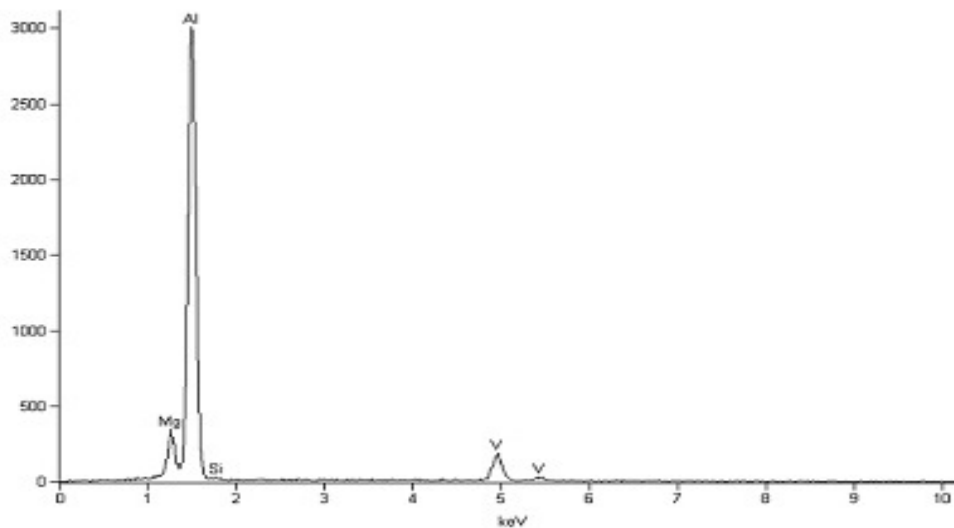
(a)



(b)

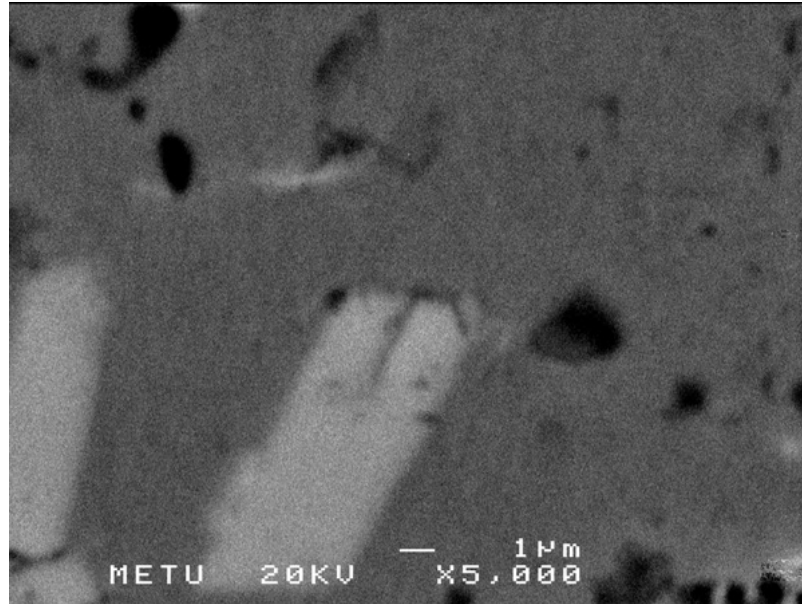
Figure 4.13 SEM micrographs of B3; (a) showing the cracked $\text{Al}_{13}\text{Fe}_4$ intermetallics, (b) showing possible Mg_2Si or $\text{Al}_{13}(\text{Fe}, \text{V})_3\text{Si}$ fine white dispersoids.

An interesting microstructure is observed in the cross sections of the flat products of both B2 and B3. Both microstructures show high intermetallic phase density through the centerline of the cross section probably due to effect of segregation during solidification between the rolls. SEM and optical micrographs of this region revealed an interesting phase different that Al-Fe intermetallics. EDX analysis of the phase showed a high Mg and V content, the intermetallic phase is characterized as $V_2Mg_3Al_{18}$ by X-ray Diffraction methods. Optical and SEM micrographs and EDX analysis is given in Figure 4.14, 4.15.

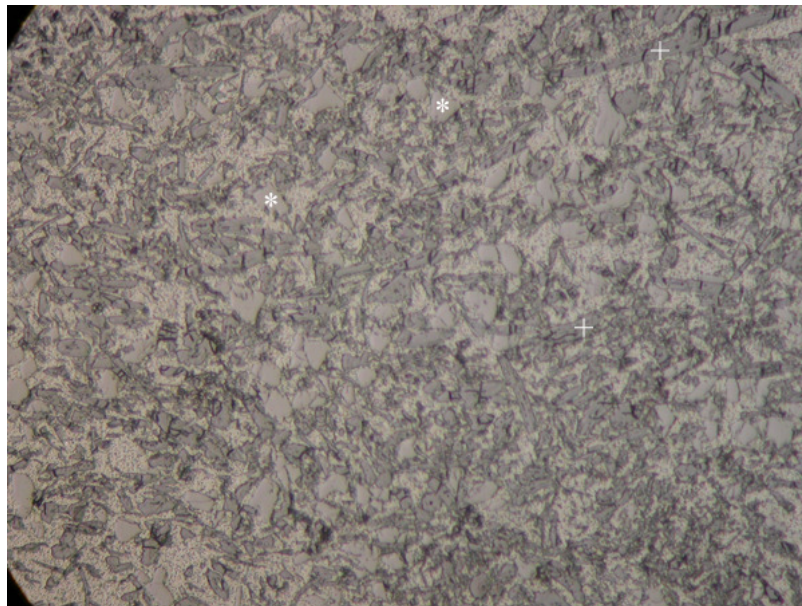


<i>Element</i>	<i>Weight Conc %</i>	<i>Atom Conc %</i>
<i>Mg</i>	5.37	6.31
<i>Al</i>	80.82	85.51
<i>Si</i>	0.96	0.98
<i>V</i>	12.85	7.20

Figure 4.14 EDX analysis of $V_2Mg_3Al_{18}$ intermetallic phase



(a)



(b)

Figure 4.15 (a) Backscattered SEM image of B3 specimen showing $V_2Mg_3Al_{18}$ intermetallic phase. (b) Typical optical micrograph of cross section of B2 and B3 specimens showing $V_2Mg_3Al_{18}^*$ and $Al_{13}Fe_{4+}$ intermetallics in X500 magnification.

4.1.2 X-Ray Diffraction Results

X-ray diffraction study is done for characterization of the suspected phases in specimens obtained from each set-up design stage since the changes in processing parameters affect the existence of secondary phases.

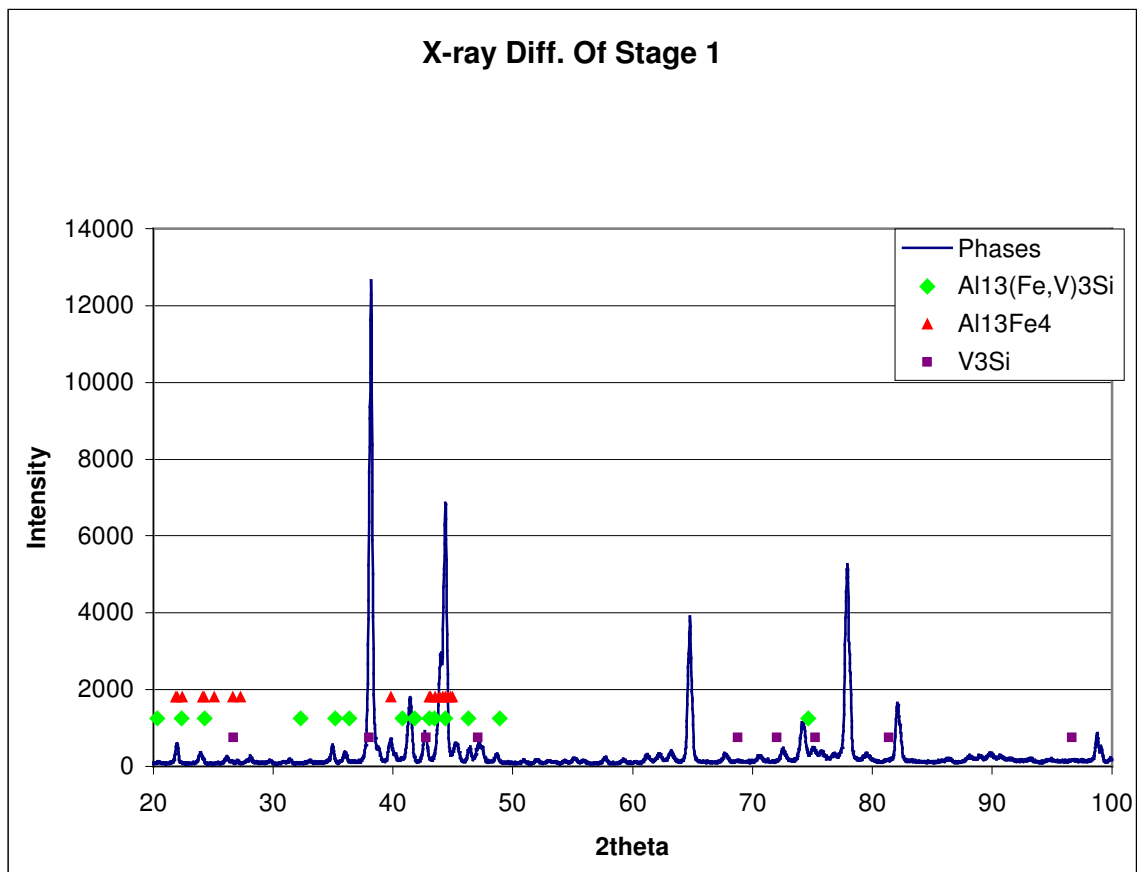


Figure 4.16 X-ray diffractogram of the specimen produced in the 1st design stage, showing characterized phases; $\text{Al}_{13}(\text{Fe}, \text{V})_3\text{Si}$, $\text{Al}_{13}\text{Fe}_4$ and V_3Si .

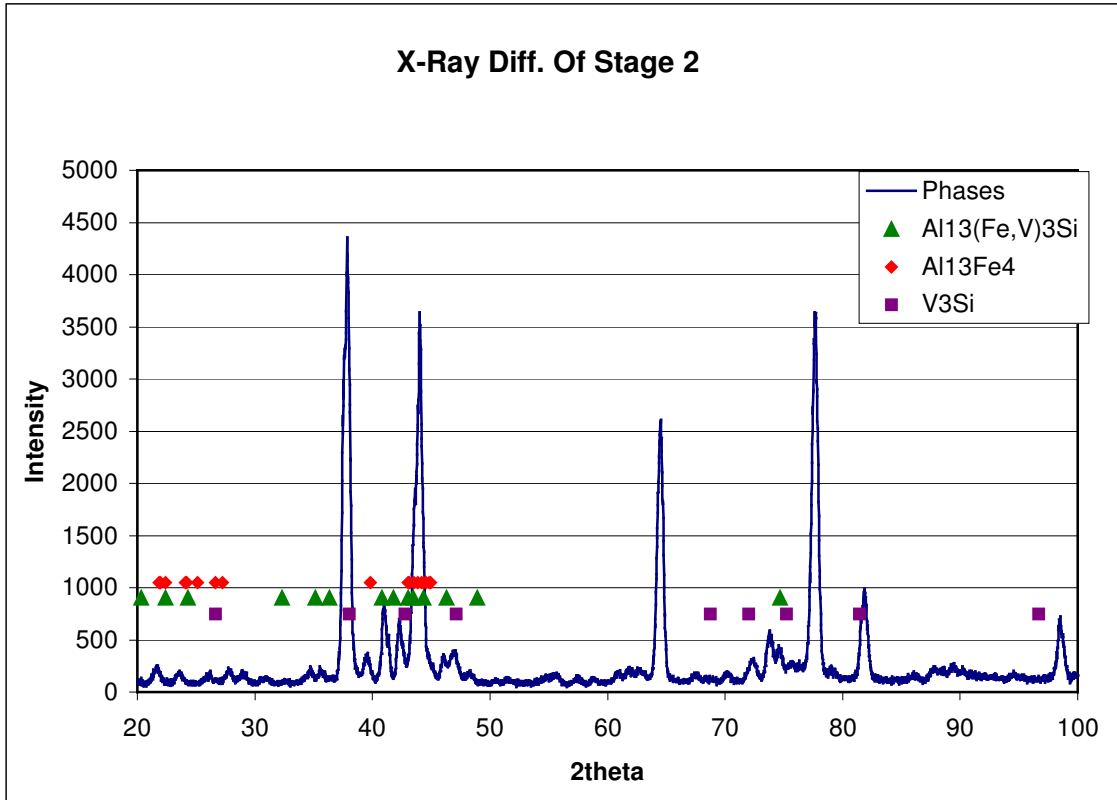


Figure 4.17 X-ray diffractogram of the specimen produced in the 2nd design stage, showing characterized phases; Al₁₃(Fe, V)₃Si, Al₁₃Fe₄ and V₃Si.

In the specimens of the first and second design stage the phases that are characterized are; the bcc Al₁₃(Fe, V)₃Si silicide phase having the lattice parameter a: 1.260 nm, the monoclinic Al₁₃Fe₄ phase having the lattice parameters as a: 1.548nm b: 8.083nm c: 1.247nm and the cubic V₃Si phase having the lattice parameter of a: 0.472nm.

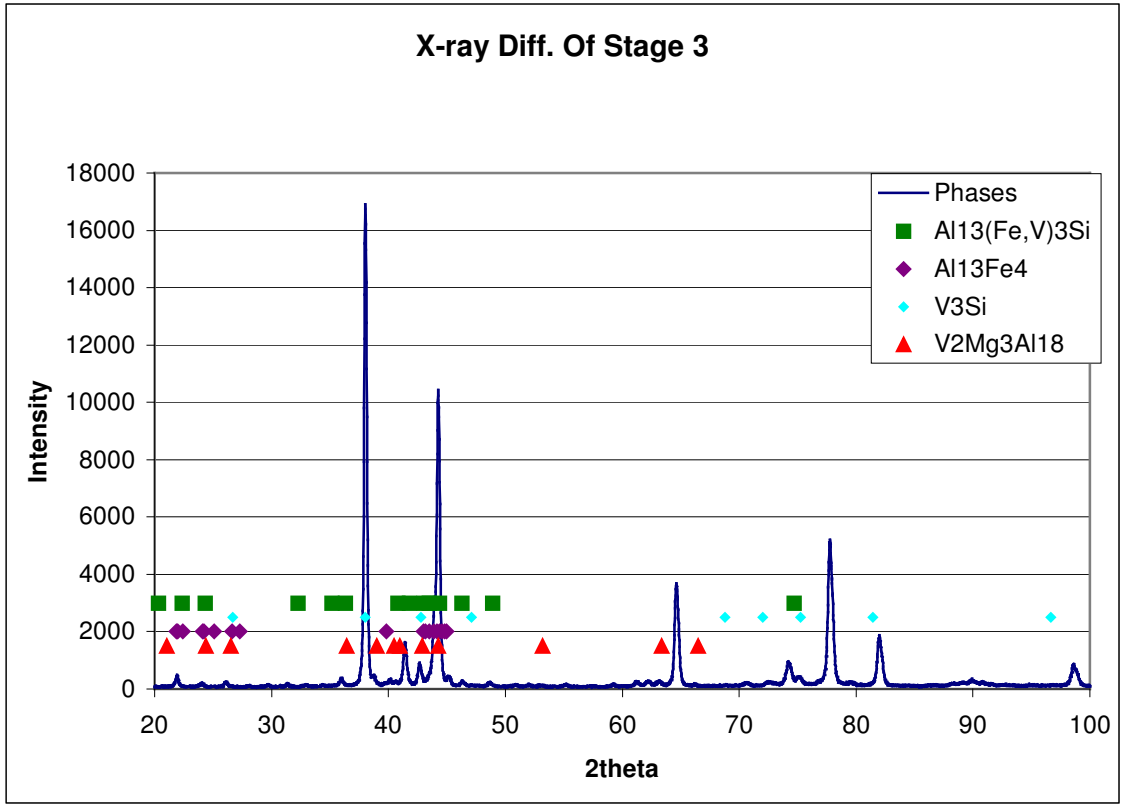


Figure 4.18 X-ray diffractogram of the specimen produced in the 3rd design stage, showing characterized phases; $\text{Al}_{13}(\text{Fe}, \text{V})_3\text{Si}$, $\text{Al}_{13}\text{Fe}_4$, $\text{V}_2\text{Mg}_3\text{Al}_{18}$ and V_3Si .

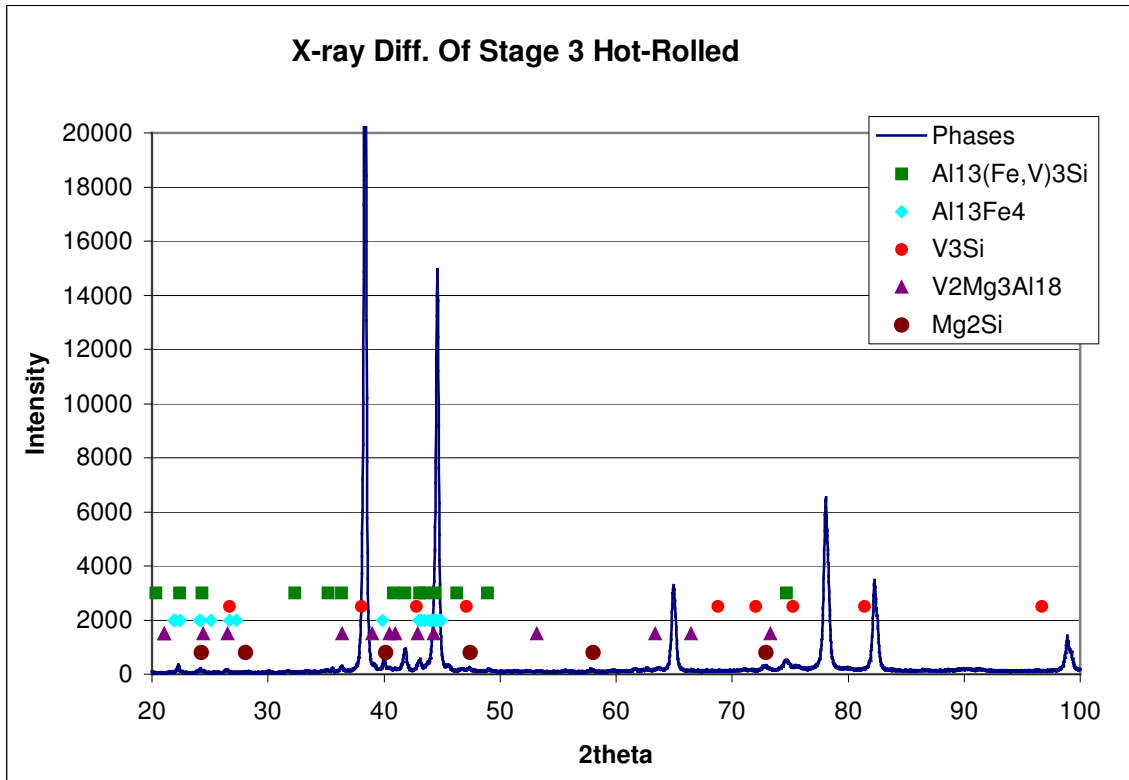


Figure 4.19 X-ray diffractogram of the specimen produced in the 3rd design stage and hot-rolled, showing characterized phases; Al₁₃(Fe, V)₃Si, Al₁₃Fe₄, V₂Mg₃Al₁₈, V₃Si and Mg₂Si.

One can conclude from the above X-ray diffractograms that the amount of V₃Si is decreased in the 3rd design stage and it does not exist in the hot-rolled specimen. Moreover a new phase is characterized in the diffractograms of 3rd stage and hot rolled specimen as V₂Mg₃Al₁₈, which is in agreement with the SEM study results. X-ray diffractogram of the hot rolled specimen also shows the possible presence of the Mg₂Si phase.

4.2 Mechanical Test Results

4.2.1 Three Point Bending Test Results

Three point bending test is applied to the specimens from the design stage that the continuous flat products are obtained, which are designated as B1 and B2 before. Maximum bending stress is measured by 0.002 offset method since the bending theory is applicable only in elastic deformation. Flexural strength values obtained are tabulated below in Table 4.2.

Table 4.2 Three point bending test results of B2 and B3.

Specimen	Result1 (MPa)	Result2 (MPa)	Result3 (MPa)	Maximum Flexural Strength (MPa)
B1 (watercooled)	161.24	207.84	227.11	198.73
B2 (air cooled)	266.26	271.83	254.54	264.21
Theoretical Tensile Strength of the Al-Fe-V-Si alloy is 462 MPa [1].				

Flexural strength values are below the expected theoretical level, this probably because of the considerable amount of porosity and the inhomogenities present in the specimens, discussed in microscopic examination section.

One can conclude from the results in Table 4.2 that the flexural strength of B2 is significantly higher than that of B1. When the microstructures of these specimens are concerned B1 features fine and rod like band shaped $\text{Al}_{13}\text{Fe}_4$ intermetallics while in B2 these intermetallics have become rounded as a result of the cooling rate achieved. Therefore, it can be said that growth of $\text{Al}_{13}\text{Fe}_4$ intermetallics into rod like band shaped morphology degrades mechanical properties so critical care should be given to the control of intermetallic morphology by the verification of cooling rate.

4.2.2 Tensile Test Results

Tensile test is applied to specimens from the continuously formed air cooled B2 and the continuously formed air cooled and further hot rolled B3. All tested specimens are cracked in the elastic region and no plastic deformation is observed when theoretical tensile behavior of the alloy is concerned it is seen that Al-Fe-V-Si alloy should represent a plastic deformation and ultimate tensile strength value about 462 MPa. [1]. Therefore, the results obtained in this study can be examined as yield strength values while these values are still significantly below the theoretical values 413 MPa.[1]. This insignificance in tensile strength test values is probably caused by poor specimen preparation. Although significant tensile strength values are not reached, elongation results are still valuable for comparison. As it can be seen from the below figure %elongation value thus ductility is decreased after hot rolling. The lower strength value that is observed in hot-rolled specimen is unexpected and probably caused because of the cracking of the intermetallics. The tensile test results are given in Table 4.3. One of the stress-strain diagrams is given in the Appendix B.

Table 4.3 Tensile strength and %elongation values of B2 and B3

Specimen	Result 1 (MPa - %elongation)	Result 2 (MPa - %elongation)	Result 3 (MPa - %elongation)	Average Fracture Strength (MPa)	Average % elongation
B2 (Air-cooled)	162.72 – 6.35	107.54 – 5.95	122.48 – 6.66	130.91	6.32
B3 (Hot- rolled)	96.32 – 4.09	83.27 – 3.79	91.35 – 4.06	90.31	3.98
Theoretical Tensile Strength of the Al-Fe-V-Si alloy is 462 MPa [1].					

4.2.3 Hardness Test Results

Hardness test of the specimens from all previously classified design stages such that A1, A2, A3, B1, B2, B3, is conducted by using the Brinell Hardness Scale (HB). Ultimate tensile strength (UTS) is also estimated from the average Brinell hardness values. Hardness test results are given in Table 4.4.

Table 4.4 Brinell Hardness test results.

Specimen	A1	A2	A3	B1	B2	B3
1	125	112	92	102	102	92
2	89	116	89	121	71	92
3	102	125	125	109	105	89
4	130	130	89	116	99	92
5	121	140	112	140	102	92
6	102	135	99	145	102	92
7	121	125	125	99	99	92
8	116	121	116	109	105	89
Average Hardness (HB)	113.25	125.50	105.88	117.63	98.13	91.25
Standart Deviation (HB)	13.17	8.76	14.50	15.83	10.47	1.30
Average UTS (MPa)	402.04	445.53	375.86	417.57	348.34	323.94
Standart Deviation (MPa)	46.75	31.10	65.48	56.20	47.17	4.61
Theoretical Tensile Strength of the Al-Fe-V-Si alloy is 462 MPa [1].						

Ultimate tensile strength values obtained from the hardness test are closer to the theoretical values contrary to the tensile and three point bending results. Therefore, one can conclude that by the spray rolling set-up designed in this study, aimed mechanical strength values are achieved by microstructural development but improvements in macro-scale is still needed to be made in the further studies.

Examination of the hardness results revealed that the A2 and B1 specimens, which are cooled in water, have higher hardness values than A3 and B2 specimens that are cooled in air. When the microstructures are considered they feature greater band shaped intermetallics instead of round intermetallics in A3 and B2, which contributed to hardness. However, it should be considered that the band shaped intermetallics caused early fracture in bending test.

When hardness distribution is taken into account, the uneven distribution is observed in A1, A2, A3 and B1 specimens. In B2 specimen the homogeneity of hardness and microstructure is observed with an exception of the transient liquid phase region, discussed in microscopical results section also featured a low hardness value of 71 HB. It is clear that this region can be avoided by control of process parameters, since in hot rolled B3 specimen hardness and microstructure is observed to become more homogeneous which can be derived from the decrease in the standard deviation in the hardness. The decrease in the hardness of the hot rolled specimen is probably due to the cracking of the intermetallics that are observed in the SEM studies.

4.3 True Density Measurement Results

True densities of two specimens from B1 (spray rolled) and B3 (hot rolled after spray rolling) are measured by helium pycnometer and compared in Table 4.5.

Table 4.5 True Density Measurement Results

Specimen	Temperature (°C)	Weight (g)	Volume (cc)	Density (g/cc)
B1-a	25.9	1.1824	0.3787	3.1223
B1-b	25.9	1.2685	0.4129	3.0724
B3-a	26.1	1.2423	0.3752	3.3115
B3-b	26.1	1.3224	0.3848	3.4362

According to the measured true density results, it can be seen that the density is increased after hot rolling, therefore one can conclude that the porosity is decreased after hot rolling of the spray rolled product.

CHAPTER 5

CONCLUSIONS

1. It is observed that molten metal flow rate directly affects the atomization of the melt, concurrently the refinement of the microstructure is dependent on the atomization, and therefore the refinement of the microstructure depends on the atomization conditions before the spray rolled product is solidified between the rolls.
2. The cooling rate just after the deposition over the rollers and during the solidification of the spray rolled strip, significantly affects the growth rate of the $\text{Al}_{13}\text{Fe}_4$ intermetallics hence their morphologies.
3. In low cooling rates monoclinic $\text{Al}_{13}\text{Fe}_4$ intermetallics having rod like band shaped morphologies are formed. The larger intermetallics contribute to hardness values while it is observed that they degrade the flexural strength, when the cooling rate is increased they become finer and rounded showing an increase in the flexural strength.
4. Microstructural features are directly affected by the change in process parameters, which contribute to the processing conditions. Therefore microstructural evaluation is a useful tool for assessing process parameters.

5. SEM EDX and XRD study of the spray rolled Al-8Fe-1.7V-8Si alloy revealed an extraordinary phase characterized as V_3Si having rounded morphology, which is formed as a result of the high Si content in the alloy.
6. SEM EDX and XRD study of the spray rolled Al-8Fe-1.4V-1.8Si alloy revealed a extraordinary phase characterized as $V_2Mg_3Al_{18}$ having rounded morphology and an average size of $10\mu m$.
7. Hot rolling of the spray rolled specimens resulted in a homogeneous microstructure thus a homogeneous hardness distribution and a significant decrease in the porosity.
8. In the further hot rolling of the spray rolled flat product, band shaped $Al_{13}Fe_4$ intermetallics are cracked, resulting a decrease in hardness values and degrading the mechanical properties. It is concluded that hot rolling parameters should be revised.
9. One of the spray rolled products exhibit an Aluminum rich zone featuring very slight amount of intermetallics. It is formed during spray rolling as a result of transient liquid formation and segregation of Fe, V and Si atoms during solute rejection from that zone. The hardness of the zone is measured to be 71HB, which is very low compared to the rest of the product.

CHAPTER 6

SUGGESTIONS FOR FUTURE WORK

1. The as-spray rolled flat product formed in the developed spray rolling set-up exhibit the desired microstructural features and homogeneous distribution of the second phase particles. However, a considerable amount of porosity is observed and it is also shown that it could be removed by applying further hot rolling. Another drawback is the bended structure of the as-spray rolled alloy sheet. Integration of a hot twin rolling stage to the present set-up, in which the alloy strip is allowed to be rolled just after production is believed to enhance the properties of the end product.
2. The integrated further hot rolling stage will allow the deformation of the product just after solidification, therefore it may avoid the cracking of the intermetallics since the deformation is applied during the growth of the intermetallic phases.
3. In this study, it is observed that when different cooling mediums i.e. water, air; are introduced just after the production of the spray rolled strip, different microstructures are obtained. Therefore, it is suspected that the cooling rate after spray rolling may affect the growth of the intermetallics. For the further studies, it is suggested that this conclusion could be examined by measuring the temperature of the as-spray rolled strip and comparing it with the decomposition temperature data of the alloy which could be obtained from DSC study.

REFERENCES

1. Aluminum and Aluminum Alloys, ASM Specialty Handbook, ASM International, Ohio (1993)
2. R.E. Sanders, Jr., G.J. Hildeman, D.L. Lege, Contract F33615-77-C-5086 Report, U.S. Air Force Mat. Lab. (1979)
3. G.J. Hildeman , R.E. Sanders, Jr., U.S. Patent 4,379,719.
4. Alloys CU78 and CZ42 for Elevated Temp. Applications, Wrought P/M Alloys, Aluminum Company of America. (1979)
5. P.S. Gilman, M.S. Zedalis, J.M. Peltier, S.K. Das, Rapidly Solidified Aluminum, Transition Metal Alloys for Aerospace Applications. (1989)
6. Rapidly Solidified Aluminum Al-Fe-V-Si Alloy, Alloy Dig., FVS812, Allied Signal Inc. (1989).
7. I.G. Palmer, M.P: Thomas, G.J. Marshall, Dispersion Strengthened Aluminum Alloys, Y.W. Kim, W.M. Griffith, Ed., TMS, (1988), 217-242.
8. D. J. Skinner, R. L. Bye, D. Raybould, A. M. Brown, Scripta Metall., 20 (1986) 867-872.

9. M. Zedalis, D. J. Skinner, *Journal of Metals*, 39 (7) (1987) A46-A46.
10. S. Lee, D. Y. Lee, N. J. Kim, *Mat. Sci. and Eng.* A147 (1991) 33-44.,
11. R. Hambleton, H. Jones, W.M. Rainforth, *Mat. Sci. and Eng.* A304-306 (2001) 524-528.
12. E.J.Lavernia, J.D.Ayers, T.S.Srivastava, *Int. Mater. Rev.* 37 (1) (1992) 1-44
13. D.J. Skinner, Y.-W. Kim, W. M. Griffith, TMS, Warrendale, PA, (1988) 181.
14. S.K. Das, L.A. Davis, *Mater. Sci. Eng.* 98 (1988) 1.
15. P.S. Gilman, S.K.Das, A Metal Powder Report Conference Luzern, MPIF, APMI, Princeton, NJ (1988) 27.1
16. K.L.Sahoo, C.S.Sivaramakrishnan, *J. Mater. Process. Technol.* 135 (2003) 253-25
17. K.L.Sahoo, C.S.Sivaramakrishnan, A.K. Chakrabarti *J. Mater. Process. Technol.* 112 (1) (2001) 6-11
18. A.R.E. Singer, *Metals and Materials*, 4 (1970) 246.
19. A.R.E. Singer, *Journal of the Inst. Metals*, 100 (1972) 185.
20. T.S. Daughery, *Powder Metallurgy*, 2 (1968) 342.

21. R.G. Brooks, Leatham A.G., Coombs J.S., Moore C., *Metallurgy and Metal Forming* 2 (1977) 100-102.
22. A.R.E. Singer, U.K. Patent 1,262,471 (1972)
23. B. Williams, *Metal Powder Report*, 10 (1980) 464-466.
24. R.K. Dube, *Powder Metallurgy International*, 14 (1982) 108.
25. R.G. Brooks, Leatham A.G., Coombs J.S., Moore C., *Powder Metallurgy*, 2 (1977) 100-102.
26. A.R.E. Singer, *Metal Powder Report*, 3 (1986) 223-226.
27. R.W. Evans, Leatham A.G., R.G. Brooks, *Powder Metallurgy*, 28(1) (1985) 13-20.
28. P.S. Grant, W.T. Kim, B.P. Bewlay, B. Cantor, *Scripta Metallurgica*, 28 (1989) 1651-1656.
29. E.J. Lavernia, G.V. McKewan, N.J. Grant, *Proc. Annu. Powder Metal. Conf. In Prog. Pow. Met.* 42 (1986) 457-478.
30. M. Gupta, F. Mohammed, E.J. Lavernia., *Metal. and Cera. Matrix Comp. Proc. Model. Mech. Behv. TMS* (1990) 91-106.
31. B.P. Bewlay, B. Cantor, *Mater. Sci. Eng. A* 118 (1989) 207.

32. E. Gutierrez, , E.J. Lavernia, G. Trapaga, J. Szekely, N.J. Grant, Metallurgical Transactions, 20A (1989) 71-85.
33. E.J. Lavernia, International Journal of Rapid Solidification, 5 (1989) 47-85.
34. P. Mathur, D. Apelian, A. Lawley, Acta Metallurgica, 37(2) (1989) 429-443.
35. E.J. Lavernia, T. Ando, N.J. Grant, Proc. 1st Int. Conf. On Rapidly Sold. Mater. San Diego CA, (1986) 29-44.
36. J. Marinkovich, F. Mohammed, J.R. Pickens, E.J. Lavernia, Journal of Metals, 41(9) (1989) 36-41.
37. K. Ogata, E.J. Lavernia, G.Rai, N.J. Grant, Int. Journal of Rapid Solidification, 2(1) (1986) 21-35.
38. V.C.Srivastava, R.K. Mandal, S.N. Ojha, Mater. Sci. And Eng. A383 (2004) 14-20
39. S.Marcus., C.Cui , U. Fritsching, Mater. Sci. And Eng. A 383 (2004) 166-174
40. C.Cui, F. Cao, Q.Li, J. Mater. Process. Technol. 137 (2003) 5-9
41. H. Bessemer, US Patent No. 49,053 (1865).
42. Ben Q. Li, JOM 47 (1995) 29.
43. L.H. Schwartz, Adv. Mater. Process. 147 (6) (1995) 104.

44. G.S. Cole, A.M. Sherman, *Mater. Charact.* 35 (1995) 23
45. J.R. Dieffenback, A.E. Mascarini, *JOM* 45 (1993) 16.
46. C.B. Burger, A.K. Gupta, P.W. Jeffrey, D.J. Lloyd, *Mater. Charact.* 35 (1995) 23.
47. M. Yun, S. Lokyer, J.D. Hunt, *Mater. Sci. Eng. A* 280 (2000) 116.
48. K.M. McHugh, J.P. Delplanque, S.B. Johnson, E.J. Lavernia, Y. Zhou, Y. Lin, *Mater. Sci. Eng. A* 383 (2004) 96-106.
49. K.L. Sahoo, S. Das, B.S. Murty, *J. Non-Cryst. Sol.* 334&335 (2004) 29.
50. A. Kalkanlı, K. Menekşe, H.A. Özyurda, *Powder Met.* 48 (3) (2005) 264.

APPENDIX A

A : X-RAY DIFFRACTION CARDS OF THE CHARACTERIZED PHASES

Table A.1 X-ray card of Aluminum

<p>89-2837 Quality: C</p> <p>CAS Number:</p> <p>Molecular Weight: 26.98</p> <p>Volume[CD]: 66.89</p> <p>Dx: 2.679 Dm:</p> <p>Sys: Cubic</p> <p>Lattice: Face-centered</p> <p>S.G.: Fm$\bar{3}$m (225)</p> <p>Cell Parameters:</p> <p>a 4.059 b c</p> <p>α β γ</p> <p>I/Corr: 4.10</p> <p>Rad: CuKα1</p> <p>Lambda: 1.54060</p> <p>Filter:</p> <p>d-sp: calculated</p> <p>ICSD #: 043492</p>	<p>Al</p> <p>Aluminum</p> <p>Ref: Calculated from ICSD using POWD-12++</p> <p>Ref: Otte, H.M., J. Appl. Phys., 32, 1536 (1961)</p> <div style="text-align: center;"> </div> <table style="width: 100%; border-collapse: collapse; margin-top: 10px;"> <thead> <tr> <th style="text-align: left;">2θ</th> <th style="text-align: left;">Int-f</th> <th style="text-align: left;">h</th> <th style="text-align: left;">k</th> <th style="text-align: left;">l</th> <th style="text-align: left;">2θ</th> <th style="text-align: left;">Int-f</th> <th style="text-align: left;">h</th> <th style="text-align: left;">k</th> <th style="text-align: left;">l</th> <th style="text-align: left;">2θ</th> <th style="text-align: left;">Int-f</th> <th style="text-align: left;">h</th> <th style="text-align: left;">k</th> <th style="text-align: left;">l</th> </tr> </thead> <tbody> <tr> <td>38.410</td> <td>999 *</td> <td>1</td> <td>1</td> <td>1</td> <td>64.982</td> <td>230</td> <td>2</td> <td>2</td> <td>0</td> <td>82.279</td> <td>62</td> <td>2</td> <td>2</td> <td>2</td> </tr> <tr> <td>44.647</td> <td>454</td> <td>2</td> <td>0</td> <td>0</td> <td>78.083</td> <td>227</td> <td>3</td> <td>1</td> <td>1</td> <td></td> <td></td> <td></td> <td></td> <td></td> </tr> </tbody> </table>	2 θ	Int-f	h	k	l	2 θ	Int-f	h	k	l	2 θ	Int-f	h	k	l	38.410	999 *	1	1	1	64.982	230	2	2	0	82.279	62	2	2	2	44.647	454	2	0	0	78.083	227	3	1	1					
2 θ	Int-f	h	k	l	2 θ	Int-f	h	k	l	2 θ	Int-f	h	k	l																																
38.410	999 *	1	1	1	64.982	230	2	2	0	82.279	62	2	2	2																																
44.647	454	2	0	0	78.083	227	3	1	1																																					

Table A.2 X-ray card of Al₁₃(Fe,V)₃Si

51-1193					Wavelength= 1.54056					
α-Al ₁₃ (Fe,V) ₃ Si					2θ	Int	h	k	l	
Aluminum Iron Silicon Vanadium					20.305	37	2	2	0	
					22.376	19	3	1	0	
					24.299	13	2	2	2	
					32.291	48	4	2	1	
					35.164	40	4	2	2	
					36.342	15	5	1	0	
Rad.:	λ:	Filter:	d-sp:		40.796	51	4	4	1	
Cut off:	Int.:		I/ cor.:		41.784	59	5	3	0	
Ref: Wang, J et al., Int. J. Non-Equilibrium Proc., 10, 83 (1997)					43.037	27	6	0	0	
					43.472	100	6	1	0	
					44.369	78	6	1	1	
Sys.: Cubic					46.283	37	5	4	0	
S.G.: P					48.929	20	6	3	1	
a:	12.60	b:	c:	A:	C:	74.677	19	9	4	1
α:	β:	γ:	Z:	8	mp:					
Ref: Ibid.										
Dx: 3.615					Dm: SS/FOM: F ₁₄ = (0.162, 83)					

The elements were melt-spun into ribbons, then quenched. Al92.8
 Ce0.28 Fe4.3 La0.15 Nd0.05 Pr0.02 Si1.7 V0.7. PSC: cP136. Mwt:
 544.33. Volume[CD]: 2000.38.

Table A.3 X-ray card of Al₁₃Fe₄

29-0042		Wavelength= 1.54056						C			
Al ₁₃ Fe ₄		2 θ	Int	h	k	l	2 θ	Int	h	k	l
Aluminum Iron		11.985	2	2	0	0	35.065	3	1	3	1
		12.476	16	1	1	0	35.379	3	4	2	1
		13.565	22	1	1	1	35.524	4	4	2	3
		14.894	4	0	0	2	36.357	2	2	2	3
		15.449	6	1	1	1	36.480	3	2	2	4
Rad.: CuK α λ : 1.54056 Filter: d-sp: Calculated		20.845	3	1	1	2	37.538	2	0	2	4
Cut off: Int.: Calculated I/lor.:		21.852	29	2	0	2	37.883	6	1	3	2
Ref: Smith, D., Yu, Penn State Univ., University Park, PA, USA.		21.983	35	2	0	3	38.049	5	3	3	0
ICDD Grant-in-Aid, (1975)		22.421	40	0	0	3	38.870	6	3	3	2
		22.949	8	4	0	1	39.563	3	5	1	2
		23.229	3	0	2	1	39.837	17	1	3	3
Sys.: Monoclinic S.G.: C2/m (12)		24.105	28	4	0	0	41.503	3	3	3	3
a: 15.489 b: 8.083 c: 12.476 A: 1.9162 C: 1.5435		24.205	32	4	0	2	41.764	10	1	1	5
α : β : 107.70 γ : Z: 24.2 mp:		25.099	53	2	2	0	42.401	10	5	1	5
Ref: Black, P., Acta Crystallogr., 8, 43 (1955)		26.651	28	0	2	2	43.015	75	6	2	0
		27.266	30	2	2	1	43.145	100	6	2	3
		27.559	7	4	0	3	43.516	38	2	0	6
		28.605	3	2	0	3	43.871	26	6	0	2
Dx: 3.840 Dm: 3.770 SS/FOM: F ₃₀ = 155(.0028 . 70)		28.756	4	2	0	4	44.164	85	0	2	5
		30.053	3	0	0	4	44.346	83	4	2	3
		31.452	2	5	1	2	44.576	62	4	2	5
		32.839	2	4	2	0	44.808	62	0	4	0
Peak height intensity. Calculated density for 24 Fe + 76.8 Al.		33.731	2	5	1	3	44.949	46	5	3	2
Al ₃ Fe type. PSC: mC101.64. To replace 2-1213. Mwt: 142.19.		34.952	3	6	0	2	45.209	7	3	1	6
Volume[CD]: 1488.02.											

2 θ	Int	h	k	l
45.550	16	5	3	0
45.681	5	1	1	6
46.655	3	5	3	3
46.888	13	8	0	2
47.138	8	1	3	4
47.557	3	3	3	3
49.867	2	6	2	5
50.454	4	2	4	3
50.670	5	0	4	3
50.931	3	4	4	1
51.277	2	5	3	2
51.522	4	4	4	0

ICDD © 2002 JCPDS-International Centre for Diffraction Data. All rights reserved
PCPDFWIN v. 2.3

Table A.4 X-ray card of Mg₂Si

		Wavelength= 1.5405981				
35-0773		2 θ	Int	h	k	l
Mg ₂ Si		24.242	41	1	1	1
Magnesium Silicon		26.071	12	2	0	0
		40.122	100	2	2	0
		47.434	15	3	1	1
		49.677	2	2	2	2
Rad.: CuK α	λ : 1.540598	58.030	13	4	0	0
	Filter: Graph Mono	63.835	6	3	3	1
	d-sp: Diff.	65.700	3	4	2	0
Cut off: 17.7	Int.: Diffract.	72.903	21	4	2	2
	I/Corr.:	78.120	4	5	1	1
Ref: Natl. Bur. Stand. (U.S.) Monogr. 25, 21, 86 (1984)		86.636	4	4	4	0
		91.698	2	5	3	1
Sys: Cubic	S.G.: Fm3m (225)	93.380	<1	6	0	0
a: 6.35119(16)	b:	c:	A:	C:		
			100.182	3	6	2
α :	β :	γ :	Z: 4	mp:		
			105.371	1	5	3
Ref: Ibid.			107.116	<1	6	2
			114.345	1	4	4
			120.033	1	5	5
			122.015	<1	6	4
Dx: 1.988	Dm:	SS/POM: F ₁₉ = 140(.0071 . 19)				

Color: Dark blue
 Peak height intensity. The mean temperature of data collection was 23.7 C. The sample was obtained from CERAC, Incorporated, Milwaukee, Wisconsin, USA. It contained a small amount of MgO. CAS #: 22831-39-6. Spectrographic analysis (wt.%, CERAC, Incorporated): 0.12 Fe; 0.05 Al; 0.01 Mn; 0.001 Ag, Ca, Cr, Cu, Ti. $\sigma(I_{obs}) = \pm 0.02$. Ca F2 type. Silicon used as an internal stand. PSC: cF12. To replace 1-1182 and 34-458. Mwt: 76.70. Volume[CD]: 256.19.

Table A.5 X-ray card of V₃Si

19-1405		Wavelength= 1.54056				i
V ₃ Si	2 θ	Int	h	k	l	
Vanadium Silicon	26.667	20	1	1	0	
	38.033	40	2	0	0	
	42.780	100	2	1	0	
	47.097	60	2	1	1	
	55.006	<5	2	2	0	
Rad.: CuK α λ : 1.5418 Filter: Ni Beta d-sp: Debye-S. 114.6	62.119	5	3	1	0	
Cut off: Int.: I/lor.:	68.766	20	2	2	2	
Ref: Ziegler, Met. Div., Argonne National Laboratory, Argonne, Illinois, USA, Private Communication, (1965)	72.030	30	3	2	0	
	75.232	30	3	2	1	
	81.419	20	4	0	0	
	93.678	10	4	2	0	
Sys.: Cubic S.G.: Pm3n (223)	96.683	20	4	2	1	
a: 4.7253 b: c: A: C:	99.801	10	3	3	2	
α : β : γ : Z: 2 mp:	122.879	40	5	2	0	
Ref: Ziegler, Downey, Trans. Am. Inst. Min. Eng., 227, 1407 (1963)	126.394	20	5	2	1	
	134.586	20	4	4	0	
	143.792	<5	5	3	0	
	155.992	20	6	0	0	
Dx: 5.694 Dm: 5.670 SS/FOM: F ₁₉ = 16(0.047, 25)	165.143	30	6	1	0	

Chemical analysis (wt.%): V 74.8, Si 25.2, Cr3 Si type. PSC: cPB. To replace 8-347. Mwt: 180.91. Volume[CD]: 105.51.

Table A.6 X-ray card of $V_2Mg_3Al_{18}$

40-1153		Wavelength= 1.5418				
V2Mg3Al18		2 θ	Int	h	k	l
Aluminum Magnesium Vanadium		10.476	25	1	1	1
		20.172	20	3	1	1
		21.057	15	2	2	2
		24.398	5	4	0	0
		26.536	1	3	3	1
Rad.: CuK α	λ : 1.5418	Filter:	d-sp: Guinier			
Cut off:	Int.:	l/lor.:				
Ref: Kerimov, K., Dunaev, S., Sljusarenko, E., J. Less-Common Met., 133, 297 (1987)		34.733	5	4	4	0
		36.404	30	5	3	1
		36.923	8	4	4	2
		39.002	25	6	2	0
		40.479	60	5	3	3
		40.962	100	6	2	2
Sys.: Cubic		S.G.: Fd3m (227)				
		42.889	15	4	4	4
a: 14.61(1)	b:	c:	A:	C:		
		44.278	30	7	1	1
		53.186	10	6	6	0
α :	β :	γ :	Z: 8	mp:		
Ref: Ibid.		56.327	1	8	4	0
		59.301	1	6	6	4
		63.345	5	9	3	3
		66.479	15	10	2	2
		73.284	20	8	8	0
Dx: 2.813	Dm:	SS/FOM: F ₁₉ = 30(.0162 , 39)				

Al18 Cr2 Mg3 type. Germanium used as an internal stand. PSC: cF184. Mwt: 660.47. Volume[CD]: 3118.53.

APPENDIX B

B: SAMPLE STRESS VS STRAIN GRAPH OF B2 SPECIMEN

Table B.1 Stress ve Strain graph of B2 specimen

